TEL AVIV UNIVERSITY
The Iby and Aladar Fleischman Faculty of Engineering
The Zandman-Slaner School of Graduate Studies

ROBOTIC MANIPULATION OF THIN OBJECTS WITHIN OFF-THE-SHELF PARALLEL GRIPPERS WITH A VIBRATION FINGER

A thesis submitted toward the degree of
Master of Science in Engineering

by

Noam Nahum

September 2022

TEL AVIV UNIVERSITY
The Iby and Aladar Fleischman Faculty of Engineering
The Zandman-Slaner School of Graduate Studies

ROBOTIC MANIPULATION OF THIN OBJECTS WITHIN OFF-THE-SHELF PARALLEL GRIPPERS WITH A VIBRATION FINGER

A thesis submitted toward the degree of
Master of Science in Engineering

by

Noam Nahum

This research was carried out at Tel Aviv University
in the School of Mechanical Engineering
Faculty of Engineering
under the supervision of Dr. Avishai Sintov
and

September 2022

Acknowledgments

I would like to thank my advisor and supervisor Dr. Avishai Sintov, for full support throughout the research, increasing motivation, creating a learning and quiet atmosphere, pushing forward for success and prosperity. Your guidance and accompaniment along the way has advanced me and brought me a great deal of knowledge in my acadameic path.

In addition, I would like to acknowledge the best group I could ask to work with, my dear friends and lab co-workers at ROBTAU Lab: Itamar Mishai, Nadav Kahanowich, Osher Azulay, Anton Gurevich, Eran Bamani, Omer Keinan, Maxim Monastirsky, Alon Mizrahi and Inbar Ben-David. I would like also to wish best of luck to Oron Binyamin and Raz Beck in continuing research this subject. Thanks to my family: Ronen, Meirav, Ido and Yoav, for your endless support along the way. My final, biggest thanks go to my fiancee, May, for always supporting, believing and motivating me to achieve my goals and have no limits.

Abstract

An in-hand manipulation refers to robots interactions with the objects they hold. It includes how the robot perceives, controls and manipulates objects. Such interactions require the planning and design of complex systems. This topic is one of the most researched topics in the field of robotics. There are various methods for manipulate objects using multiple degrees of freedom robotic hand. however, Common parallel grippers are suffering from the lack of DOF and are limited to closing on an object without the ability for intrinsic in-hand manipulation. Nevertheless, parallel grippers are widely used due to their simplicity and low-cost while relying on extrinsic capabilities for manipulating the object. In this work, a simple and low-cost mechanism is proposed for augmenting a parallel gripper with intrinsic in-hand manipulation abilities. A novel vibration-based finger was proposed where an off-the-shelf eccentric rotating mass motor along with a simple rotary actuator apply directional movement forces on a grasped thin object. The motion is based on the *stick-slip* phenomenon and exerted with no exposed moving parts. Along with the mechanism, a simple control law is proposed to manipulate the object to desired position goals and along paths. Furthermore, the ability to manipulate various objects is demonstrated. Experimental results show the ability to manipulate an object with accuracy of less than 2 mm. The experiments demonstrate the merits of the approach granting in-hand manipulation capabilities, that previously were not possible, to any parallel gripper.

This work was accepted and submitted by Ramot as a PCT (International) patent application under **HIGH RESOLUTION ROBOTIC FINGERS. https://ramot.org/technologies/high-resolution-robotic-fingers**

The work in this thesis was published in:
Noam Nahum and Avishai Sintov. Robotic manipulation of thin objects within off-the-shelf parallel grippers with a vibration finger. *Mechanism and Machine Theory*. 177:105032, 2022.

Table of Contents

List of Figures

List of Tables

1 Introduction

In-hand manipulation is the ability to hold and move an object within one hand. In-hand manipulation skills are essential to many tasks used by human as handwriting, grasping objects, move an object inside hand. It is easy to take for granted actions in the hand that are performed by a person on a daily basis. Examples for such are: working with tools that require holding a different object, touching the phone, taking money out of the wallet etc. These basic operations are not obvious when it comes to robotic grippers. Yet, in-hand manipulation capabilities of robotic hands are an important feature for efficient interaction with the environment. While dexterous robotic hands, such as the Shadow and the Allegro hands, are very capable, they have complex structure with many degrees-of-freedom (DOF) and, therefore, require agile sensory feedback, sophisticated control and planning to achieve robust manipulation [24]. Hence, these hands are highly expensive and not accessible for practical applications such as assembly lines or medical procedures. Parallel jaw grippers, on the other hand, are widely used due to their simplicity, durability and low cost. They can precisely grasp almost any object of the same scale and, therefore, are ubiquitous in industrial application of material handling [23]. However, jaw grippers normally have only one DOF for opening and closing the jaws. Hence, they do not have independent in-hand manipulation capabilities. The most common manipulation approach for jaw grippers is pick-and-place where the object is placed on a surface and picked up again in a different grasp configuration [62]. However, the picking and placing can be slow and demands a large surface area around the robot.

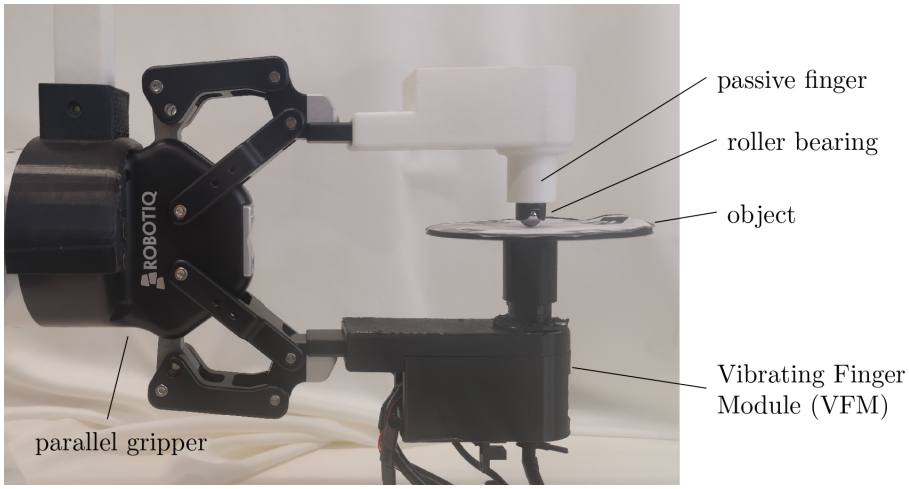

Figure 1.1: Prototype of the Vibratory Finger Manipulator (VFM) installed on an off-the-shelf parallel gripper.

This work explores the use of vibration for in-hand manipulation. In this thessis, a novel mechanism termed *Vibratory Finger Manipulator* (VFM) is proposed. The VFM module can potentially augment the capabilities of any generic off-the-shelf parallel jaw gripper and enable it to perform in-hand manipulation of thin objects (Figure 1.1). The VFM is a simple and affordable vibration-based mechanism which can easily be integrated onto any parallel gripper. The motion principle is based on the *stick-slip* phenomenon where the application of vibrations enables active control of friction [5]. Such approach enables the generation of a propagation force onto an object in contact. Hence, this effect is employed using a low-cost vibration motor along with a rotary actuator to steer the force towards the required direction. Along with the mechanism, a dynamic analysis of the proposed system is provided. Furthermore, with vision-based object configuration feedback, the ability to control the motion and manipulate the object to desired goals is shown. The proposed mechanism has applications in, for example, precise manipulation of thin surgical knifes in medical procedures, robot insertion of plastic cards (e.g., credit cards) and key manipulation.

To summarize, the contributions of this work are as follows. First, a novel vibration-based mechanism is proposed that augments the capabilities of any standard off-the-shelf parallel gripper. The mechanism is composed of simple and low-cost hardware. Standard parallel grippers are unable to perform intrinsic in-hand manipulation. With the addition of such simple mechanism, parallel grippers are given the ability to perform in-hand manipulation of thin objects. In addition, a simple model-free controller is proposed to manipulate a grasped object to desired goal positions. The proposed system is tested and

analyzed over a set of different objects. To the best of the authors' knowledge, our work is the first to combine vibration motors to in-hand manipulation for robotic hands.

2 Related work

State-of-the-art for in-hand manipulation with parallel grippers (that does not involve picking and placing) is commonly divided to extrinsic and intrinsic dexterity [3].

2.1 Extrinic dexerity

Extrinic dexerity is the ability to compensate for the lack of DOF using external supports, such as friction, gravity and contact force.

2.1.1 Dynamic Manipulation

Extrinsic dexterity compensates for the lack of gripper DOF and involves actions of the entire robotic arm for either pushing the object against an obstacle [17, 9] or performing dynamic manipulation such as pivoting [58, 59, 43, 46, 14] and throw-and-catch [44]. Another work by [16] shows various re-grasp actions by three-finger grippers where all of the actions are open loop while relying on external resources. In another work [30], an asymmetric gripper is proposed (Multi Modal Gripper). The gripper consists of a modular thumb with varying degrees of passive compliance and a dexterous, tendon-driven forefinger that can produce either under-actuated or fully-actuated behaviors. This methods relies on two actuators and basic open loop control action and requires change in the passive finger for applying different movement of in-hand manipulation.

2.1.2 Gravity-based manipulation

A different approach leverages gravity to control slippage between the fingers of the parallel gripper [13]. For instance, Costanzo [12] exploited a dual-arm system and tactile feedback to allow controlled slippage between the object and a parallel gripper. Another work using gravity [57] proposed a sliding mode controller for in-hand manipulation that

reposition a tool in the robots hand by using gravity and controlling the slippage of the tool. The slippage is controlled by varying the opening between the fingers in order to allow the tool to move to the desired angular position.

2.1.3 Friction and contact manipulation

The work of Shi et al. [41] controlled the force distribution of a pinch grasp to predict sliding directions. Similarly, Chen et al. [10] controlled the sliding velocity of an object grasped by a parallel gripper. These methods usually require grip force control and agile sensory feedback of object pose. Another approach [48] used a variable friction robotic fingers that are able to significantly change the effective coefficient of friction of their contact surface. Thus, the object is moved by changing the friction when one finger is applied as a sliding surface and the other is applied as a static surface. This method requires additional motors in the finger and thus increase mechanism complexity. Similar work in [52] presented a novel end-effector that merges the essential mechanics and control simplicity of manipulable dexterous robotics hands using active surfaces. The end-effector simulated different levels of friction and applied tangential thrust to the object in contact. In [8], a two phase gripper is presented which is designed to passively re-orient objects while picking them up using two phases of the finger-object contact geometry. This method also uses external forces such as gravity to orient the object. When it is not necessary to move or orient the object, this mechanism can change the grip point and prevent it from moving.

2.2 Intrinsic dexterity

Intrinsic dexterity is the ability of the robots hand to manipulate the object using its own DOF [15]. While jaw grippers have only one DOF, some work have been done to augment their intrinsic manipulation capabilities. Seminal work by Nagata [33] proposed six gripper mechanisms with an additional one DOF at the tip, each having an ability to either rotate or slide an object in some direction. Similarly, a passively rotating mechanism was integrated into the fingers of the gripper allowing the object to rotate between the fingers by gravity [51]. In [63], a jaw gripper tip was augmented with a two DOF transmission mechanism to re-orient and translate randomly placed screws.

In [35], a novel three-finger robot is presented inspired by a spherical parallel mechanism which is design to achieve rotation of a grasped object using three actuators. In [65], linear actuation was added along each of the two fingers to enable translation and twist of a grasped object. Similarly, a rolling mechanism was added to the gripper in [7]

in order to manipulate a flat cable. In-hand manipulation was also enabled for a minimal under-actuated gripper by employing an active conveyor surface on one finger [1]. In [50], a pneumatic braking mechanism was included to a parallel gripper in order to transition between object free-rotating and fixed phases. The above augmentation methods for parallel grippers are limited to one manipulation direction and yield bulky mechanisms that complicate the hardware. In [32], the Stewart Hand with a six DOF is presented. The mechanism consists of three parallel linkage fingers with six prismatic actuators that control manipulation. The hand demonstrated a large range of motions but suffer from high complexity. Another approach is using soft and continuum robots finger. In [54], a highly deformable 3D printed soft robot (PS robot) is presented. The hand is capable of generating complex, robust gaits on different inclines using a novel variable friction leg design. This design changes the frictional force depending on the robot posture and shape to facilitate robot locomotion. This feature is useful for grippers when grasping forces need to be adjusted to the manipulated object. In [6], an under-actuated, tendon driven, anthropomorphic manipulator with two flex-or tendons and an abduction-adduction tendon is presented. This mechanism is designed directly by experimental human precision manipulation data.

2.3 Manipulation using Vibration

The first known part manipulation with vibration was presented by Chladni during the 18th century using acoustic-based horizontally-vibrating plates [11]. Similarly, recent work used a single acoustic actuator to control the position of multiple objects on an horizontal plate simultaneously and independently [64]. In addition to acoustic vibrations, the use of mechanical excitation to generate vibrations and object manipulation has been widely researched [19, 31]. The work by Böhringer [4] analyzed the effect of plate oscillation frequency and the corresponding dynamic modes to the motion of an object. In [36], four linear actuators were used to generate various velocity fields across an horizontal plate. Breguet and Clavel [5] introduced the *Stick-Slip* actuators using piezo-elements to manipulate micro-components. Stick-slip is a phenomenon where contact between two surfaces is alternated between static (i.e., no relative motion) and kinetic (i.e., sliding relative each other) friction, and is caused by, for instance, applying vibrations. Baksys at el. [2] used one rotary actuator with a perpendicular axis to generate tangential forces that traverse an object across the plate. Most recently, Kopitca et al. [28] used a piezoelectric actuator to generate nonlinear vibration fields for gathering particles into a desired two-dimensional shape.

Not much work have combined mechanical grippers to the notion of vibration. However, vibration is extensively used in releasing micro- and nano-objects within a parallel gripper [18, 29, 20]. In [37], vibration was used to overcome the adhesion force of a vacuum gripper holding micro-objects. On the other hand, Honda [25] proposed a two finger gripper where each finger is comprised of an Eccentric Rotating Mass (ERM), a mass and two springs. Such gripper can hold an object of unknown weight and surface with the most suitable grasping force. Nakamura and Honda [34] proposed a multi-finger robotic hand where each finger has a vibration roller to allow uni-dimensional motion of a grasped object. Similarly, the work by Suzuki et al. [49] used vibration to control slippage of an object during gravity-based pivoting.

While the above works focused on manipulating arbitrary objects using vibration of an extrinsic horizontal plate, some efforts have been put to manipulate micro-robots by employing on-board vibration motors. A large effort has been put on micro-actuation techniques based on piezoelectric actuators [40, 42]. However, piezo-components are complex systems and quite expensive [56]. Hence, using the Stick-Slip principle, Vartholomeos and Papadopoulos [55] proposed to actuate a micro-robot using two simple mechanical vibration motors positioned co-linearly. Such mechanism enables precise actuation with low cost hardware. The mechanism later inspired the design of the Kilobot [38] for swarming behaviour research [39].

3 Background

3.1 Dry Friction

Dry friction is a mechanical phenomenon that occurs between surfaces, it is a force that opposes the relative lateral motion of two solid surfaces in contact. There are different types of dry friction including dynamic friction that occurs between moving surface and static friction that occurs between non-moving surface. Similarly, kinetic friction results in a force that resists the sliding or rolling of one solid object over another. On the other hand, static friction is the force that avoids object from initiating motion. This physical phenomenon plays an important role in this research as it causes movement of the objects that is gripped by the VFM.

3.1.1 Coulomb's law of dry friction

Friction force is model by the Columbus law of friction. The model will be used in this research for analyzing and modeling the movement of different objects by the VFM. The Coulombs law for dry friction is described by three major rules. The first law of Coulomb's law of dry friction states that the magnitude of the frictional force will be directly proportional to the normal load between the surfaces for a given pair of materials. The rule is described mathematically for static and dynamic friction by

$$f \leq \mu_s N \tag{3.1}$$

and

$$f = \mu_k N, \tag{3.2}$$

respectively, where N is the normal load. Scalar μ_s and μ_k are the static and dynamic coefficients of friction, respectively. The second Coulomb law describes that the magnitude of the frictional force is independent of the contact area, i.e., apparent area for a given

normal load. In addition, the third law states that the magnitude of the frictional force will be independent of the sliding velocity.

3.2 ERM Mechanism

The Eccentric rotating mass (ERM) consist of a normal DC motor with unbalanced mass connected to its shaft. Different vibration frequencies and intensities are created by spinning the offset mass at varying speeds. As a result, the motor transfers vibration to the attached device. The vibration produced by ERMs is *Driven Harmonic Vibration*. This means there is an external driving force that causes the system to vibrate at the frequency of excitation. The force of an ERM can be described by a sinusoidal wave

$$F = F_0 \sin \omega t. \tag{3.3}$$

F_0 is referred to the amplitude of the sine wave given by

$$F_0 = mr\omega^2 \tag{3.4}$$

where ω is the excitation frequency, m is the mass of the eccentric mass and r is the distance from the motor shaft to the center of the eccentric mass. For simplicity, a 1 DOF system of ERM is be presented next.

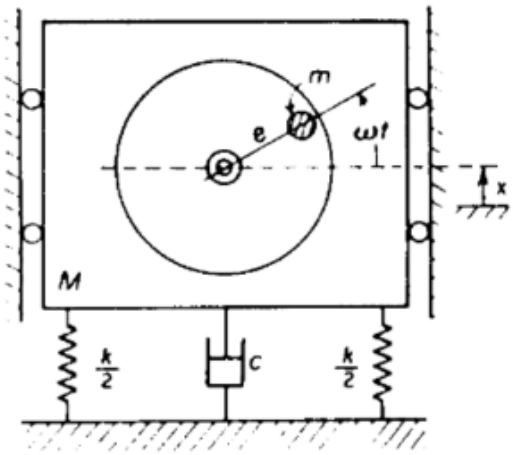

Figure 3.1: ERM of 1 DOF with a mass model.

The one DOF vibration model can be described by a mass M connected to a spring with stiffness k and damper c (Figure 3.1). The equation of motion is constructed of the

forces of these three components and the input force:

$$(M+m)\ddot{x}(t)+c\dot{x}(t)+kx(t)=F_0\sin\omega t. \tag{3.5}$$

3.2.1 Mechanical resonance

Mechanical resonance is a physical phenomenon where an external force (such as the force produced by the ERM) can drive a system to a much higher amplitude at a specific frequency. This is known as the Resonant Frequency and for equation (3.5) its equal to

$$\omega_n=\sqrt{\frac{k}{M+m}}. \tag{3.6}$$

3.2.2 Stiffness

Stiffness is the resistance of an elastic body to deflection or deformation by an applied force.

3.2.3 Damping

Damping refers to energy losses that occur in the system throughout each cycle. There are three types of damping: over-damped where the system decays without oscillation; under-damped where the system oscillates but continues to decay; and critically-damped where the system returns to zero as quickly as possible with no decays. For the 1 DOF system, the critical damping c_{cr} and damping ratio ζ is given by

$$c_{cr}=2\sqrt{k(M+m)}=2\omega_n(m+M) \tag{3.7}$$

and

$$\zeta=\frac{c}{c_{cr}}. \tag{3.8}$$

Thus, equation (3.5) becomes

$$\ddot{x}(t)+2\zeta\omega_n\dot{x}(t)+\omega_n^2x(t)=\omega_n^2\frac{F_0}{k}\sin\omega t. \tag{3.9}$$

With initial conditions of $x(0)=x_0$ and $\dot{x}(0)=v_0$, the homogeneous solution $x_h(t)$ for the non-damped system $\zeta<1$ is given by

$$x_h(t)=e^{-\zeta\omega_n t}X\cos(\omega_d t-\phi) \tag{3.10}$$

where X is the amplitude, ϕ is the frequency and ω_d is the damped natural frequency.

3.2.4 Displacement by an ERM

Consider equation (3.9), for the steady state, the homogeneous solution has no influence because it vanishes. Thus, only the particular solution has an impact on the system which is given by

$$x(t)_p = X_p \cos(wt - \phi_p) \tag{3.11}$$

where X_p is the amplitude and ϕ_p is the frequency given by

$$X_p(\omega) = \frac{F_0}{k(1-(\frac{\omega}{\omega_n}^2))^2 + (\frac{2\zeta\omega}{\omega_n})^2)} \tag{3.12}$$

and

$$\phi_p(\omega) = \arctan(\frac{\frac{2\zeta\omega}{\omega_n}}{1-\frac{\omega}{\omega_n}^2}). \tag{3.13}$$

Inserting (3.4) into (3.12), the maximum amplitude will be at the natural damped frequency of the system where $\omega = \omega_d$:

$$\omega_d = \omega_n\sqrt{1-\zeta^2}. \tag{3.14}$$

Figure (3.2) shows the normal distribution for displacement with regards to frequency.

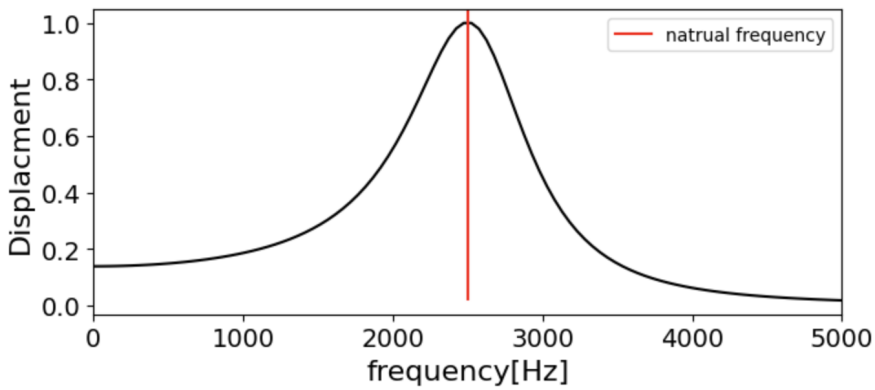

Figure 3.2: Maximum displacement will occur at the natural frequency.

3.3 Vibration of bars

3.3.1 Longitudinal vibration

Consider a uniform homogeneous elastic bar of length L, cross-section A and mass M on its free end as shown in figure 3.3. The bar mass is $m_b << M$ with constant modulus E. The bar has a constant of equivalent spring stiffness K which is equal by Hawks law to

$$K = EA/L. \tag{3.15}$$

One end of the bar is attached to a fixed wall while the other end is free. On the free edge of the bar there is an action force $P(t)$ which is equal to.

$$P(t) = C\sin(wt) \tag{3.16}$$

where w and C are the frequency and amplitude of the applied force. Using Newton's second law, and under the assumption that $m_b << M$ infinitesimal analysis along the bar will not be considered, and neglecting the damping of the bar, the equation of motion is given by

$$(m_b + M)\ddot{u} + Ku = C\sin(\omega t). \tag{3.17}$$

The natural frequency of the system is

$$\omega_n = \sqrt{\frac{(K)}{m_b + M}} = \sqrt{\frac{L(m_b + M)}{EA}}. \tag{3.18}$$

Thus, equation (3.17) is now

$$\ddot{u} + {\omega_n}^2 u = B\sin(\omega t). \tag{3.19}$$

The general solution for (3.19) is equal to

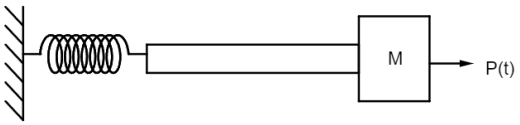

Figure 3.3: Longitudinal vibration of a beam

$$u(t) = C_1 \sin\left(\frac{EA}{ML}t\right) + C_2 \cos\left(\frac{EA}{ML}t\right) + U_p \tag{3.20}$$

where U_p is the particular solution. The homogeneous solution vanishes at the steady state. Therefore, we focus only on the particular solution:

$$U_p = A \sin \omega t + B \cos \omega t. \tag{3.21}$$

Inserting this into (3.17) yields

$$({\omega_n}^2 - \omega^2) B \cos \omega t + ({\omega_n}^2 - \omega^2) A \sin \omega t = C \sin \omega t. \tag{3.22}$$

The extraction of A and B provides

$$A = \frac{C}{\omega_n^2 - \omega^2} \tag{3.23}$$

and

$$B = 0. \tag{3.24}$$

Thus, the particular solution is now

$$U_p = \frac{C}{\omega_n^2 - \omega^2} \sin \omega t = u(t). \tag{3.25}$$

The equation presents the follows. If ω is equal to ω_n, the solution reaches infinity and the system will move in high amplitudes with high harmonic velocity:

$$\dot{u}(t) = \omega \frac{C}{\omega_n^2 - \omega^2} \cos \omega t \tag{3.26}$$

3.3.2 Transverse vibration

Consider the same uniform homogeneous elastic bar of length L, cross section A and mass M on is free end as shown in Figure 3.4. The elastic bar has moment of inertia I and stiffness K which is equal by Hooke's law to

$$K = \frac{3EI}{L}. \tag{3.27}$$

This elastic bar is exerted by an harmonic force equal to (3.16). Similar to the longitudinal

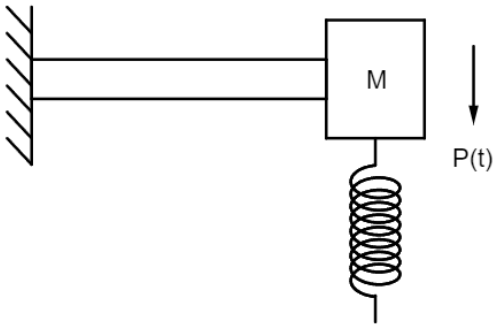

Figure 3.4: Transverse vibration of a beam.

case, the equation of motion is given by

$$(m_b + M)\ddot{u} + \frac{3EI}{L}u = B\sin(\omega t). \tag{3.28}$$

For this case, the solution will be the same like the longitudinal but with different natural frequency which is equal to

$$\omega_n = \sqrt{\frac{K}{m_b + M}} = \sqrt{\frac{3EI}{L(m_b + M)}}. \tag{3.29}$$

Applying a frequency close to the natural frequency of the two cases will help using the forces applied by the beam movement.

3.4 Slip Stick Phenomena

Stick-slip is a surfaces movement alternating between sticking to each other and sliding over each other, with a corresponding change in friction force. Stick-slip motion is caused by the difference between static friction coefficient and kinetic coefficient, and it tends to occur with slower sliding velocity and higher normal load. The above occurs because the static friction coefficient between two surfaces is larger than the kinetic friction coefficient. If an applied force is large enough to overcome the static friction, then the reduction of the friction to kinetic friction can cause a sudden jump in the velocity of movement. Thus, Stick-slip motion is generated by the repetition of "stick" and "slip".

This phenomena is explained in [53] and approximates the motion of a 1 DOF vibration system with Coulomb friction. Consider a solid body of mass m, a linear spring with stiffness k, and viscous damper with damping coefficient c as show in Figure 3.5. The object contacts a flat floor surface with a normal load W, and the floor is moving in the positive x direction with velocity V. The object is forced by friction F which is function of the relative velocity between the object and the floor $V_{rel} = V - \dot{x}$. The force is given by

$$F = \begin{cases} F_s, & |F_s| < |\mu_s W| \\ sign(V_{rel})\mu_k W, & |F| > \mu_s |W|, \end{cases} \tag{3.30}$$

where F_s is the actual static friction force, $|\mu_s W|$ is the maximum static friction, μ_s and μ_k are the static and kinetic friction coefficients. The difference between the two friction coefficients is

$$\Delta\mu = \mu_s - \mu_k > 0. \tag{3.31}$$

Despite the above equation, in our system analysis (Chapter 4), friction force will not be analyzed. Alternatively, nonlinear mapping force will be assumed which is influenced by the fabrication and speed.

3.4.1 Stick to Slip movement analysis

When the object is in the stick state, transition to slip movement will occur when the following condition is satisfied

$$m\ddot{x}(t) + c\dot{x}(t) + k\Delta x(t) > \mu_s |W|. \tag{3.32}$$

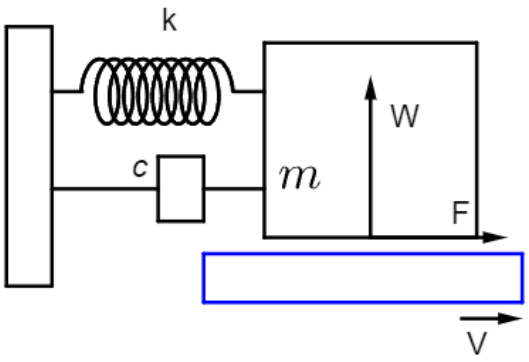

Figure 3.5: Simple 1 DOF Slip-Stick model

When object motion changes from stick to slip, maximum static friction force is exerted on the object. This maximum static friction force is suddenly released and, due to the stored elastic force displacement of the spring, the object starts slipping.

3.4.2 Slip to Stick movement analysis

When the object is in the slip state, transition to stick mode will occur when

$$m\ddot{x}(t) + c\dot{x}(t) + k\Delta x(t) = \mu_k |W|. \tag{3.33}$$

This occurs when the relative velocity is equal to zero.

3.5 Control background

3.5.1 Stability using Lyapunovs method

Lyapunov's direct method uses a physical observation of the system. If the total energy of a mechanical (or electrical) system is continuously dissipated, then the system, whether linear or nonlinear, must eventually settle down to an equilibrium point, i.e., it is stable. This means, we can use a scalar "energy like" function (Lyapunov functions) to examine the stability of the system.

Stability

The state $x = 0$ is said to be stable if, for any $R > 0$, there exists $r > 0$, such that if $|x(0)| < r$, then $|x(t)| < R$ for all $0 \leq t$. Otherwise the state point is unstable.

Positive definite function

A scalar continuous function $V(x)$ is said to be locally positive definite if $V(0) = 0$ and in a ball B_{R_0} for $x \neq 0$, then $\rightarrow V(x) > 0$. If $V(0) = 0$ and the above holds over the whole state space, then $V(x)$ is said to be globally positive definite.

Lyapunov function

If, in a ball B_{R_0}, the function $V(x)$ is positive definite and has continuous partial derivatives, and if its time derivative along any state is negative semi-definite such that $\dot{V}(x) \leq 0$, then $V(x)$ is said to be a Lyapunov function for the system.

Lyapunov theorem for global stability

Assume that there exists a scalar function $V(x)$ with continuous first order derivatives such that $V(x)$ is positive definite, $\dot{V}(x)$ is negative definite and $V(x) \rightarrow \infty$ as $|x| \rightarrow \infty$, then the equilibrium at the origin is globally asymptotically stable.

In this research, a simple controller will be implemented on the system. The stability of the system will be analyzed using direct Lyapunov method by finding Lyapunov candidate function for the system.

4 System

4.1 Method

4.1.1 Design

We leverage the ability of vibration in order to manipulate an object in contact and propose the design of the VFM module. An illustration of the VFM mechanism is seen in Figure 4.1. The VFM is composed of two actuators: an ERM motor and a rotary one. The ERM motor is positioned at the tip of the finger within a rotating shaft such that its axis is perpendicular to the shaft axis. The shaft is fabricated by 3D printing with a Polylactic-Acid (PLA) filament and rotates within three bearings to allow concentric motion with minimal friction. In addition, the rotating shaft includes a thin bending plate where its normal is perpendicular to the ERM axis. While a high second moment of area of the shaft (e.g., a circular profile) in the vibration direction would cause attenuation and loss of force magnitude, the bending plate with low second area moment routes the vibrational force in the direction of its normal and reduces attenuation.

The ERM motor and bending plate are covered be an elastic sleeve fabricated by 3D printing with an elastic polymer (Thermoplastic polyurethane). This configuration enables high vibrational forces at the finger pad in contact with the manipulated object while reducing attenuation. Due to this configuration, there may be some small angle deviations of the bending plate in its normal direction. Although some vibration force losses may exist, the deviations are significantly limited by the finger sleeve. Hence, the deviations are considered negligible and the motion of the plate tip is assumed to be horizontal. By rotating the ERM motor, harmonic force is generated on the plane perpendicular to the rotation axis. The harmonic force generates the Stick-Slip effect (explained in detail below) yielding object movement. Furthermore, the sleeve is mounted to the base of the model where a rotary actuator is connected to the shaft through a bevel gear. Using an encoder, the rotary motor can rotate the shaft and control the direction of the vibrational forces.

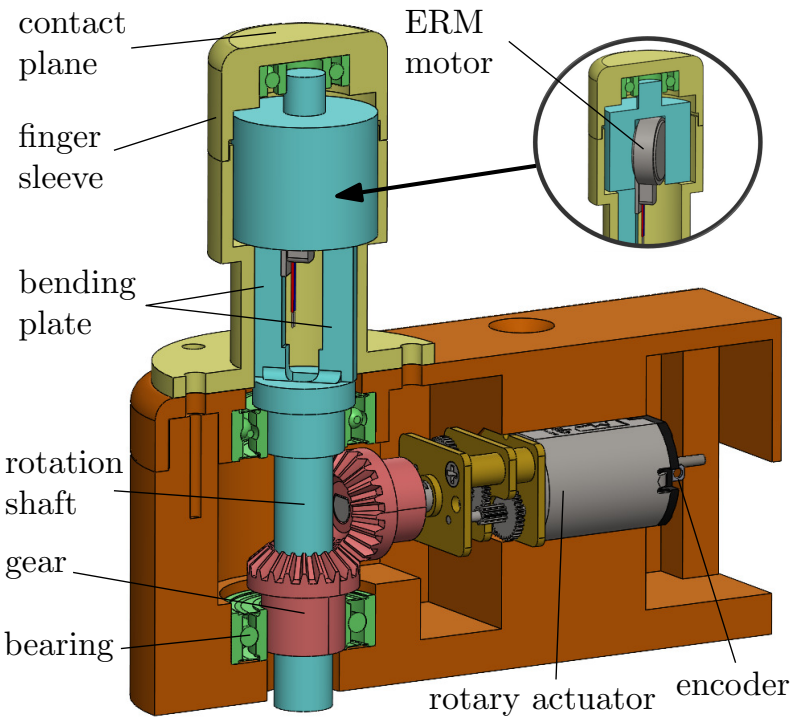

Figure 4.1: Section view of the Vibratory Finger Manipulator (VFM).

At the opposing side of the gripper, a passive finger is fixed. A roller ball bearing is positioned at the tip of the passive finger and is in contact with the object for minimal friction. Both fingers grasp the object in some initial force f_b in direction normal to the object surface. The above mechanism provides an encapsulated vibration system to manipulate an object without exterior or exposed moving components. In the following sections all analysis for the system is provide. All notation and nomenclature used throughout the work is shown in Table 4.1.

4.1.2 Dynamic Analysis

In this Section, the motion principle of the ERM motor is analyzed, based on previous work for micro-robots [55]. Then, given object $\mathcal{B}$ with mass M and inertia moment I, the dynamic effect of the mechanism on $\mathcal{B}$ is observed.

Movement force

The motion mechanism of the ERM is based on a small eccentric mass m rotated by a motor through a link of length l as shown in Figure 4.2. The rotation is assumed to be in

Table 4.1: Notation and nomenclature used throughout the paper

Symbol	Meaning	Symbol	Meaning
DOF	Degrees Of Freedom	$\mathbf{g}$	Gravitation vector
VFM	Vibratory Finger Manipulator	f_ξ, f_ζ	forces on rotation axis
ERM	Eccentric Rotating Mass	$\mathbf{f}_N$	Normal force
COM	Center Of Mass	f, f_c	Forces
RMSE	Root Mean Square Error	$\mathcal{O}$	VFM coordinate frame
f_b	Initial grasp force	$\mathbf{r}$	Object COM position
$\mathcal{B}$	Manipulated object	ϕ	Object orientation
M	Mass of manipulated object	θ	Force steering angle
I	Inertia of manipulated object	τ_f	Torsional friction torque
m	ERM mass	τ_t	Net torque
l	ERM link length	γ	Static torsional friction coef.
φ	ERM rotation angle	μ	Dyn. torsional friction coef.
ω	ERM frequency	μ_s	Static friction coef.
ξ, ζ	ERM coordinate axes	μ_k	Dynamic friction coef.
$\hat{\cdot}$	Unit vector	$\mathbf{r}_g$	COM goal position
Γ	Scalar	$\mathbf{x}, \mathbf{y}, \mathbf{z}$	State vectors

constant angular velocity (e.g., frequency) $\omega = \dot{\varphi}$ where φ is the angle of rotation. In such setting, forces exerted on the rotation axis in directions of the mechanisms coordinate axes ξ and ζ, while considering the orientation of the gripper, are given by

$$f_\xi = ml\omega^2 \cos\varphi + m(\hat{\xi} \cdot \mathbf{g}) \tag{4.1}$$

$$f_\zeta = ml\omega^2 \sin\varphi + m(\hat{\zeta} \cdot \mathbf{g}), \tag{4.2}$$

where $\hat{\xi}$ and $\hat{\zeta}$ are the axes vectors expressed in some global coordinates, and $\mathbf{g}$ is the gravitation vector. The dot products in (4.1) and (4.2) are the projection of the gravitational force on the $\hat{\xi}$ and $\hat{\zeta}$ axes, respectively.

The resulting vibrational forces described above are exerted on the grasped object. The normal force that is exerted on the object due to the ERM, dual-finger grip and gravitation is

$$f_N = f_\zeta + f_b + M(\hat{\zeta} \cdot \mathbf{g}). \tag{4.3}$$

Furthermore, force f_ξ is attenuated due to the structure of the finger, i.e., due to the elastic sleeve and bending plate. That is, the tangential force exerted on the object is

$$f = \Gamma(f_\xi) \tag{4.4}$$

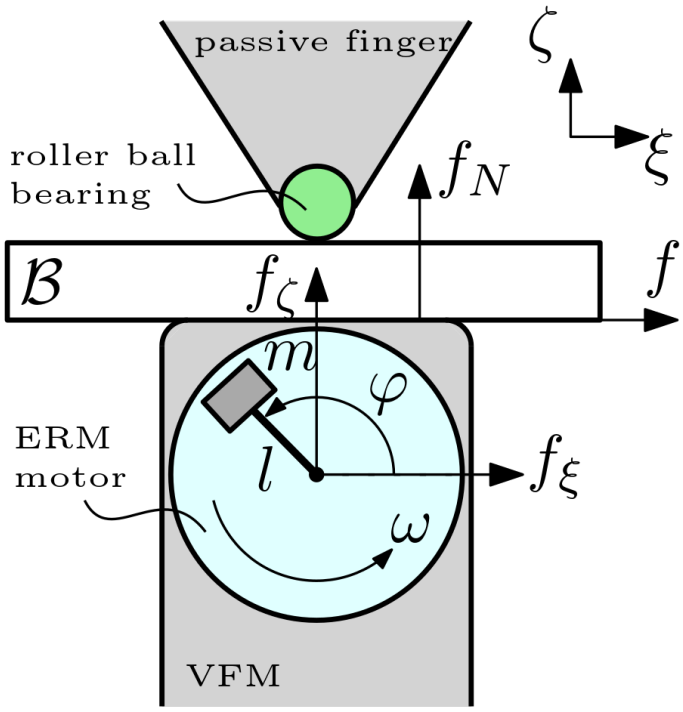

Figure 4.2: Illustration of the ERM rotation plane and the stick-slip effect on the object in contact.

where $\Gamma(\cdot)$ is some unknown non-linear map [61]. The map would reduce the amplitude of the force such that $f \leq f_\xi$ while it is difficult to evaluate because of the complex structure and fabrication process.

Object dynamic model

Coordinate frame $\mathcal{O}$ is defined to be fixed at the center of the VFM as seen in Figure 4.3. Hence, the configuration of object $\mathcal{B}$ with respect to $\mathcal{O}$ is defined by the position $\mathbf{r} = (x, y, 0)^T$ of the center-of-mass (COM) and the rotation angle ϕ about the z axis, i.e., the configuration space of the $\mathcal{B}$ is $SE(2)$. The motion of $\mathcal{B}$ occurs, therefore, on plane $x-y$ of $\mathcal{O}$. Force f from (4.4) is exerted on the object at steering angle $\theta \in [-\pi, \pi]$ with respect to the x-axis, i.e., in direction $\hat{\mathbf{f}} = (\cos\theta, sin\theta, 0)^T$. Steering angle θ is, therefore, the action input to the system which defines the desired object direction of motion. The equations of motion that describe the sliding of the object within the gripper fingers are

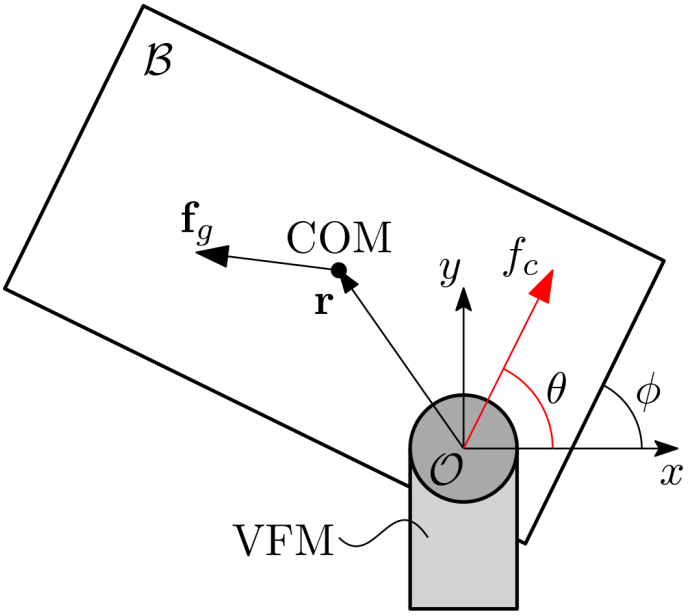

Figure 4.3: Illustration of vibration force f_c applied to object $\mathcal{B}$.

given by

$$M\ddot{x} = (f_c + f_g)\cos\theta \tag{4.5}$$

$$M\ddot{y} = (f_c + f_g)\sin\theta \tag{4.6}$$

$$M\ddot{\phi} = \frac{1}{x^2+y^2}(f_c\,(x\sin\theta - y\cos\theta) - (xf_{g_y} - yf_{g_x}) + \tau_f) \tag{4.7}$$

Vector $\mathbf{f}_g = (f_{g_x}, f_{g_y}, 0)^T$ is the projection of the gravitation force vector $M\mathbf{g}$ onto the motion plane $x-y$. That is, force $\mathbf{f}_g$ is the effect of gravitation on the planar motion and acting on the COM as seen in Figure 4.3. Scalar f_g is the operation of $\mathbf{f}_g$ along the direction of the vibration force and is given by the dot product $f_g = \mathbf{f_g}\cdot\hat{\mathbf{f}}$. Equation (4.7) is acquired from the conservation of momentum where the first term at the right hand side is the z component of the cross product $\mathbf{r}\times\hat{\mathbf{f}}$. Similarly, the second term is the z component of the cross product $\mathbf{r}\times\mathbf{f}_g$ and is the torque generated by the gravitational force. Scalar τ_f is the torsional friction at the contact point and is given by

$$\tau_f = \begin{cases} -\gamma f_N sgn(\tau_t), & |\dot{\phi}| = 0 \\ -\mu f_N sgn(\dot{\phi}), & |\dot{\phi}| > 0, \end{cases} \tag{4.8}$$

where τ_t is the net torque acting on the contact point in order to maintain static equilibrium, and $\gamma, \mu > 0$ are the static and dynamic coefficient of torsional friction [27, 45].

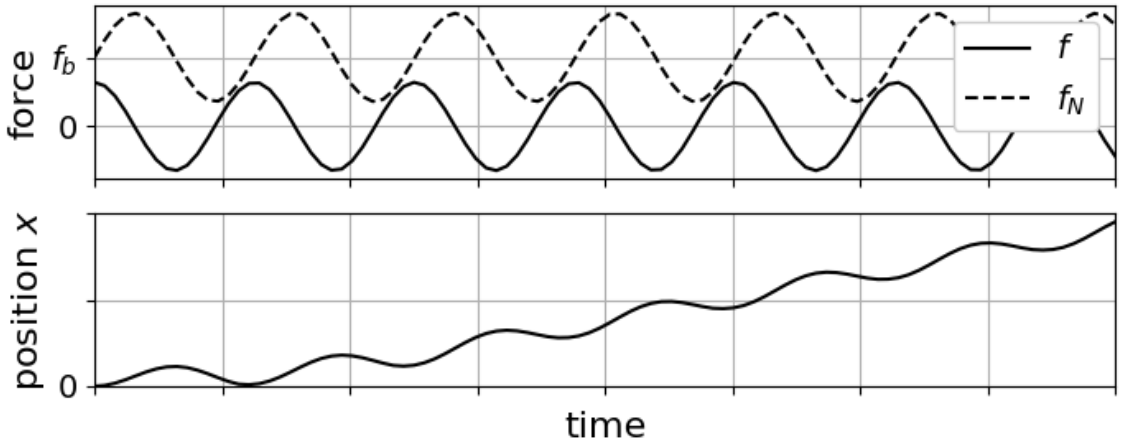

Figure 4.4: A one-dimensional example of motion: (top) Tangential and normal forces, f and f_N, applied to the object and (bottom) displacement of object along the x direction.

Force f_c is dependent of whether the object and finger are in *stick* mode (i.e., static friction) or in *slip* mode (i.e., relative motion with kinetic friction), and is given by

$$f_c = \begin{cases} f, & |f + f_g| \leq \mu_s |f_N| \\ f - \mu_k f_N, & |f + f_g| > \mu_s |f_N|, \end{cases} \tag{4.9}$$

where μ_s and μ_k are the static and kinetic coefficients of friction, respectively, between the finger and object. In the slip mode, the object will move in direction $\hat{\mathbf{f}}$, when $f_g > 0$ and f_g is assisting f_c; or when $f_g < 0$ and $|f_c| > |f_g|$. The latter case depends on the friction coefficient and grip force. Hence, inclined manipulation under the effect of gravity will be demonstrated in the experimental section.

Figure 4.4 presents a one-dimensional simulated example (i.e., solely along the x-axis) of the motion. In this example, the angular velocity ω is in the positive direction. While $f_N > f_b$, the eccentric mass is at the highest point ($\varphi = 90^\circ$) of the cycle leading to high frictional force. This is the stick phase in which the f force is applied to the object in the positive direction and, thus, generating displacement of both finger and object in the positive x direction. Similarly, when the mass is at its lowest point ($\varphi = -90^\circ$), the normal force is the lowest. When the magnitude of the normal force declines, the f force switches direction yielding relative slip between the finger and object (while the finger experiences negative displacement). Consequently, the displacement in the positive direction is larger than the negative one, leading to cumulative net displacement in the positive direction. Excitation of negative ω would force negative displacement in the same manner.

A gripper with a VFM finger has a one-DOF actuation space (i.e., steering angle θ) while the object configuration is of three-DOF (i.e., x, y and ϕ). Hence, the system is considered underactuated where the entire configuration of the arm cannot be fully controlled. The next section discusses position control of the object while maintaining constant orientation. Controlling object position along with its orientation requires manipulation planning which we leave out of the scope of this paper.

4.1.3 Control

Consider the problem of manipulating the COM of the object to a goal position $\mathbf{r}_g = (x_g, y_g, 0)^T$ relative to $\mathcal{O}$. While the control of the COM position is formulated, the position of any other point on the object can be controlled instead as will be shown in the experiments. System (4.5)-(4.7) can be formulated in the state space as

$$\dot{\mathbf{x}} = F(\mathbf{x}, \theta) \tag{4.10}$$

where $\mathbf{x} = (x_1, \ldots, x_6)^T \in \mathbb{R}^6$, $x_1 = x$, $x_2 = \dot{x}$, $x_3 = y$, $x_4 = \dot{y}$, $x_5 = \phi$, $x_6 = \dot{\phi}$,

$$F(\mathbf{x}, \theta) = \begin{pmatrix} x_2 \\ \frac{f_a}{M}\cos\theta \\ x_4 \\ \frac{f_a}{M}\sin\theta \\ x_6 \\ \frac{1}{M({x_1}^2+{x_3}^2)}(f_c(x_1\sin\theta - x_3\cos\theta) - (x_1 f_{g_x} - x_3 f_{g_y}) + \tau_f) \end{pmatrix}, \tag{4.11}$$

and $f_a = f_c + f_g$. While having a sinusoidal behaviour, force f_c is assumed to be constant and positive for control purpose. Hence, force f_c pushes the object in direction defined by control input angle θ. Further, the state vector can be decomposed as $\mathbf{x} = (\mathbf{y}, \mathbf{z})^T$ where $\mathbf{y} = (x_1, x_2, x_3, x_4)^T \in \mathbb{R}^4$ and $\mathbf{z} = (x_5, x_6)^T \in \mathbb{R}^2$ correspond to linear and angular motion of the object, respectively. Therefore, system (4.10) can now be represented as

$$\dot{\mathbf{y}} = Y(\mathbf{y}, \theta) \tag{4.12}$$

$$\dot{\mathbf{z}} = Z(\mathbf{z}, \theta) \tag{4.13}$$

where $Y : \mathbb{R}^4 \times \mathbb{R} \to \mathbb{R}^4$ and $Z : \mathbb{R}^2 \times \mathbb{R} \to \mathbb{R}^2$.

Consider the following Lyapunov candidate function [47]

$$V(\mathbf{y}) = \frac{1}{2}(x_1 - x_g)^2 + \frac{1}{2}(x_3 - y_g)^2 + \frac{1}{2}x_2^2 + \frac{1}{2}x_4^2 \tag{4.14}$$

where $V(\mathbf{y}) > 0$ for $\mathbf{y} \neq \mathbf{y}_g$ with $\mathbf{y}_g = (x_g, 0, y_g, 0)^T$ as the goal $\mathbf{y}$-state. Substituting (4.12) to the time derivative of V gives

$$\dot{V}(\mathbf{y}) = (x_1 - x_g)x_2 + (x_3 - y_g)x_4 + x_2\frac{f_a}{M}\cos\theta + x_4\frac{f_a}{M}\sin\theta. \tag{4.15}$$

Having $\lambda < \frac{M}{f_a}$ for some $\lambda > 0$ and choosing

$$\cos\theta = -\lambda(x_1 - x_g), \;\; \sin\theta = -\lambda(x_3 - y_g) \tag{4.16}$$

or

$$\tan\theta = \frac{y_g - x_3}{x_g - x_1}, \tag{4.17}$$

we get that

$$\dot{V}(\mathbf{y}) = \left(\frac{f_a}{M} - \lambda\right)(x_2\cos\theta + x_4\sin\theta). \tag{4.18}$$

Since $\dot{x}\cos\theta > 0$ and $\dot{y}\sin\theta > 0$ (or $sgn(\dot{x}) = sgn(\cos\theta)$ and $sgn(\dot{y}) = sgn(\sin\theta)$), it must be that

$$\dot{V}(\mathbf{y}) \leq 0. \tag{4.19}$$

According to partial stability theorem [60], system (4.10) is $\mathbf{y}$-stable. Therefore, by applying controller

$$\theta = \arctan\left(\frac{y_g - x_3}{x_g - x_1}\right), \tag{4.20}$$

with $\lambda > \frac{f_a}{M}$, and as long as $x_2, x_4 \neq 0$, the Lyapunov function decreases and the system is driven to $\mathbf{y}_g$.

The $\mathbf{y}$-stability of the system means that control law (4.20) will take sub-system $Y(\mathbf{y}, \theta)$ to position $(x_g, y_g, 0)^T$. However, applying the control to (4.7) yields

$$\ddot{\phi} = \frac{1}{M({x_1}^2 + {x_3}^2)}\left[f_c((x_1 y_g - x_3 x_g) - (x_1 f_{g_x} - x_3 f_{g_y})) + \tau_f\right]. \tag{4.21}$$

Hence, the object would rotate by the effect of the controller and sub-system $Z(\mathbf{z}, \theta)$ cannot be controlled. Nevertheless, rotation would not occur if the object is at a position satisfying $xy_g - yx_g = 0$ and $\tau_f = x_1 f_{g_x} - x_3 f_{g_y}$. That is, rotation will not occur if the object

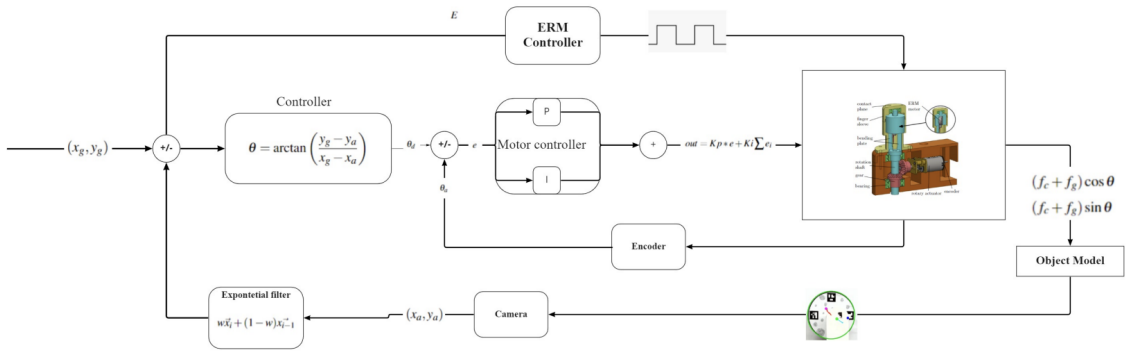

Figure 4.5: Control architecture for controlling the center of mass.

moves on a line connecting the COM and the goal, and when the object is grasped tight enough by the normal force f_N to resist gravitational torque (this is easily done by applying sufficient grip force f_b and demonstrated in the experiments). In such case, motion is exerted towards or away from the COM, no torque is applied on the object and, therefore, the object will not rotate. If no rotation is desired when moving to some goal $(x_g, y_g, 0)^T \neq (0,0)$, controlling the motion through the COM is proposed. That is, an intermediate goal $(0,0)$ is added prior to moving to $(x_g, y_g, 0)^T$ and, thus, moving only on rotation-free lines. Figure 4.5 shows the control diagram block used in this system.

5 Experiments

5.1 Hardware

A prototype of the VFM was built as described in Section 4.1.1. The VFM includes an ERM vibration motor 10×3.4 *mm* by Pololu. We note that physical parameters of the ERM such as m and l are not specified by the manufacturer. The VFM was further installed on a Robotiq 2F-85 parallel gripper while the gripper is mounted on a Kinova Gen3 arm as seen in Figure 5.2 which is capable of lifting 4.5kg payload. It is noted that the VFM can be installed on any parallel gripper with no regards to its closing mechanism. Also, the Robotiq 2F-85 gripper cannot provide feedback about the closing force f_b and, therefore, the gripper was closed manually on the object to some arbitrary force by using a custom Python library. Data acquisition, control and communication were implemented using a customized mechatronic system. To begin with, the control of the VFM is done by using a micro-controller which controls the motor direction in the low level using PI controller. The controller also calibrates the system at each power up. Next, we must pose sensing capabilities in order to communicate with the environment. This is done using a web camera which is positioned on top of the system to track the ArUco [21] markers on the moving object. The camera provides feedback stream of object position and orientation in real-time and in frequency of 30 Hz. Aruco markers provide, within the working distance of the experiment, position and orientation errors of approximately 1.5 *mm* and 1°, respectively [22, 26].

5.2 Software

The software have been developed in two separate platforms. The first platform is used for developing the micro controller software using STM32 Nucleo MCU. This board is used to acquire data from the sensors, control motor position, activate the vibration motor and calibrate the initial state of the motor using an optic switch. This first low level

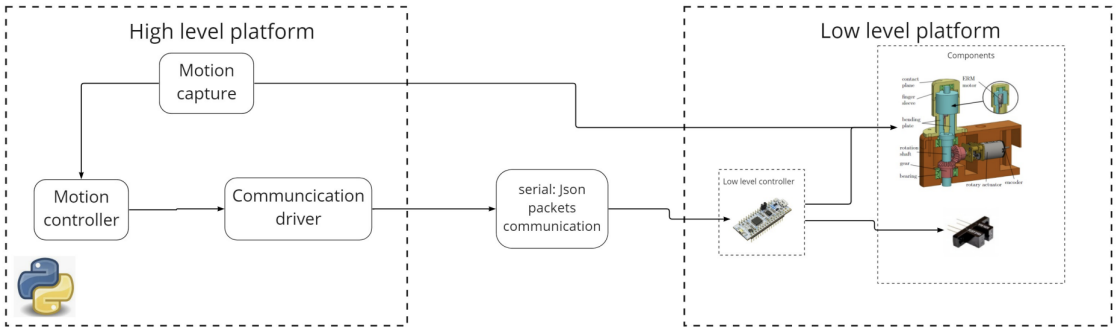

Figure 5.1: Hardware and software architecture.

platform is responsible for receiving the data from the high level platform. The high-level platform was developed in Python for different packages. The first package is responsible for opening a communication pipeline to the low level platform. The second package is responsible for acquiring information from the camera. Finally, the third package consists of the control method for object position Figure 5.1 shows the hardware and software architectures.

5.3 Experiment procedure

We first analyze the manipulation of a circular thin object printed with PLA of weight 14.84 grams and thickness 2 mm. The manipulation of other objects is later observed. Experiment videos can be seen in the following link: `https://youtu.be/P2lIUu4Uv2w`.

5.3.1 Mechanism Analysis

The behaviour of the mechanism with regards to certain parameters is initially observed including vibration frequency, gripper inclination and various manipulated objects. For each of the tests, object mean velocity over a sequence of 200 random steps exerted by the VFM is reported. A sequence of positions was recorded and the velocity was computed by second order backward differentiation. First, velocity of the object is observed with regards to the frequency of the ERM. Figure 5.4 shows results in which object velocity clearly increases with higher frequency. Hence, one can also tune the frequency in order to control moving velocity. Note that the velocities also depend on the attenuation of the gripper structure derived from fabrication, material and geometry.

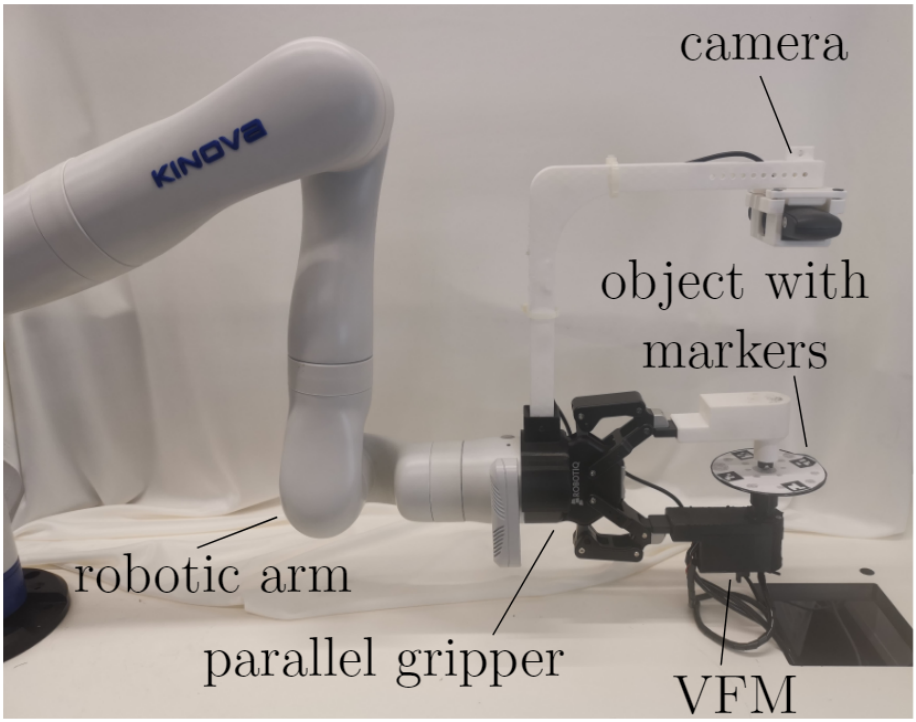

Figure 5.2: Experimental setup where the VFM is mounted on a Robotiq parallel gripper.

Next, the mean velocity of the object with regards to gripper inclination is analyzed. For such, random paths were recorded while changing the gripper angle using the robotic arm. Figure 5.5 shows results for mean and standard deviation object velocities with regards to the inclination angle. A rather low grip force f_b was applied on the object by the gripper between angles 0° to 25°. Above 25° inclination, the object began to slide due to gravitation. Hence, an higher gripping force was applied to increase friction. For inclination angles larger than 60°, the gripper failed to generate continuous motion of the object as the vibration force was not strong enough. Having a stronger ERM should allow working in steeper angles. It is noted that rotation due to gravitation when not applying vibration was not observed and static equilibrium was maintained by τ_f (as discussed in Section 4.1.3). Hence, grip force f_b was sufficient while not interfering with vibration control. Figure (5.3) shows the force balance between gravity and vibration force.

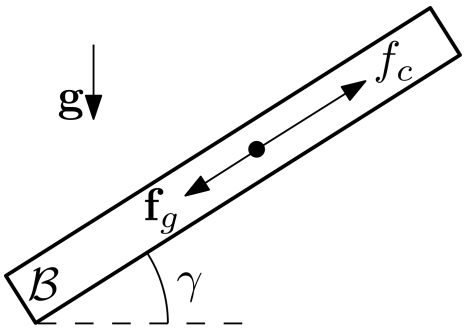

Figure 5.3: Inclination by angle γ of object $\mathcal{B}$ where vibration force f_c must overcome gravitation force $\mathbf{f}_g$. Force $\mathbf{f}_g$ is the projection of the gravitation force vector $M\mathbf{g}$ onto the motion plane of the object.

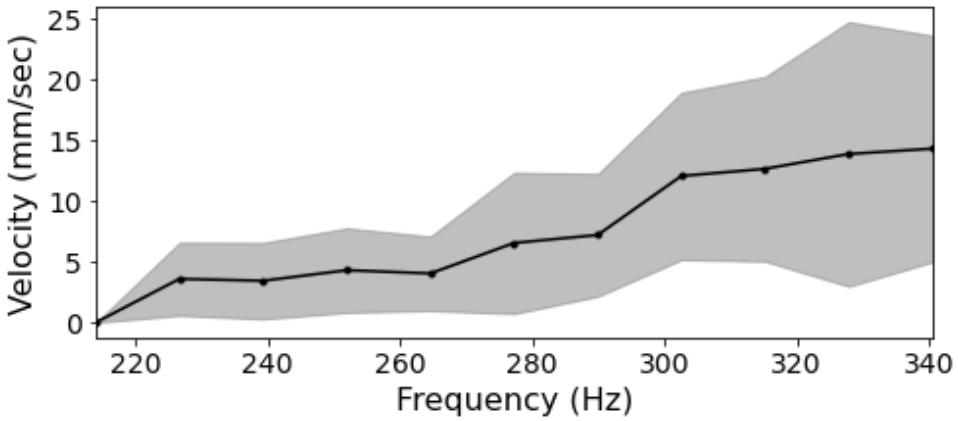

Figure 5.4: Mean object velocity with regards to the frequency of the vibration motor.

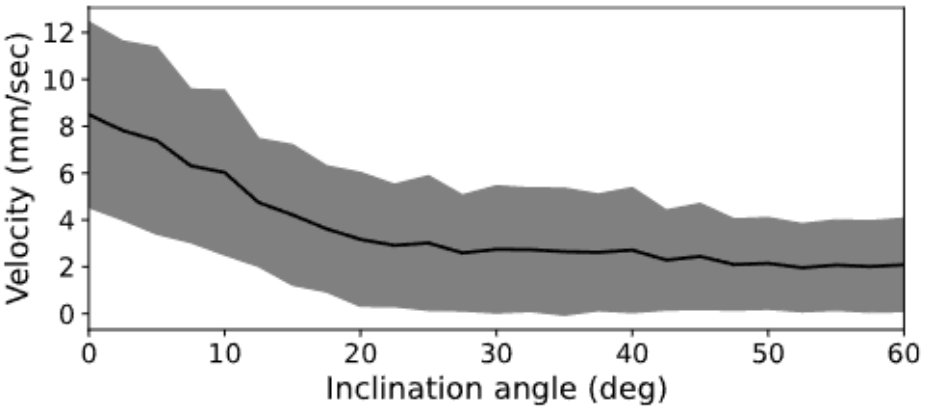

Figure 5.5: Mean object velocity with regards to the inclination angle of the gripper.

Table 5.1: Performance parameters of controller (4.20) **directly to the goal or through the origin**

		Direct	via origin
Mean error	(mm)	1.58±0.49	1.47±0.54
Mean angle change	(deg)	11.40±15.62	4.27±4.34
Mean path length	(mm)	63.75±42.86	66.55±36.48

5.3.2 Control Evaluation

In this section, the use of control law (4.20) is experimented to manipulate the object to desired goal positions. The control of the COM motion directly to desired goals and through the origin are tested. Table 5.1 shows performance parameters for the two control strategies over 100 trials. For each trial, a desired goal was randomly chosen and motion was initiated from the reached point of the previous trial. The COM is declared to reach the target if it is within 2 mm of the goal position. This distance tolerance is defined based on the position measurement error of the system described above. When the COM reaches the current goal, vibration is terminated and motion stops instantly due to stick attenuation. Controlled motion is then applied to the next random goal. Results show that the mean final error is low and less than 2 mm for both methods. While relatively low, the error is significantly affected by the resolution of the ArUco marker tracking as discussed above, and can be reduced in future work with a designated sensing alternative. Note also that explicit knowledge of friction parameters between the gripper and objects are not required for the controller to reach desired targets.

Moving through the origin is shown to reduce the mean angle change by approximately 62%. When moving directly to the goal, torques are exerted on the object yielding a curved path as seen in Figure 5.6. On the other hand, control through the origin constrains forces to be nearly along a line passing through the origin leading to lower torques on the object. Hence, the paths are less curved as seen in Figure 5.7. Evidently, Table 5.1 shows that the mean lengths of paths passing and not passing through the origin are approximately similar. Position responses corresponding to manipulations in Figures 5.6 and 5.7 are seen in Figures 5.8 and 5.9, respectively.

Using the control law, path tracking was also implemented along small-sized paths. Each path was discretized to 60 points. Tracking was performed with a moving intermediate goal point, i.e., a simple "follow-the-carrot" scheme, where the next intermediate point is set to be the goal once the object reaches the current one. Table 5.2 presents path sizes and average Root Mean Square Error (RMSE) for tracking rectangular and circular

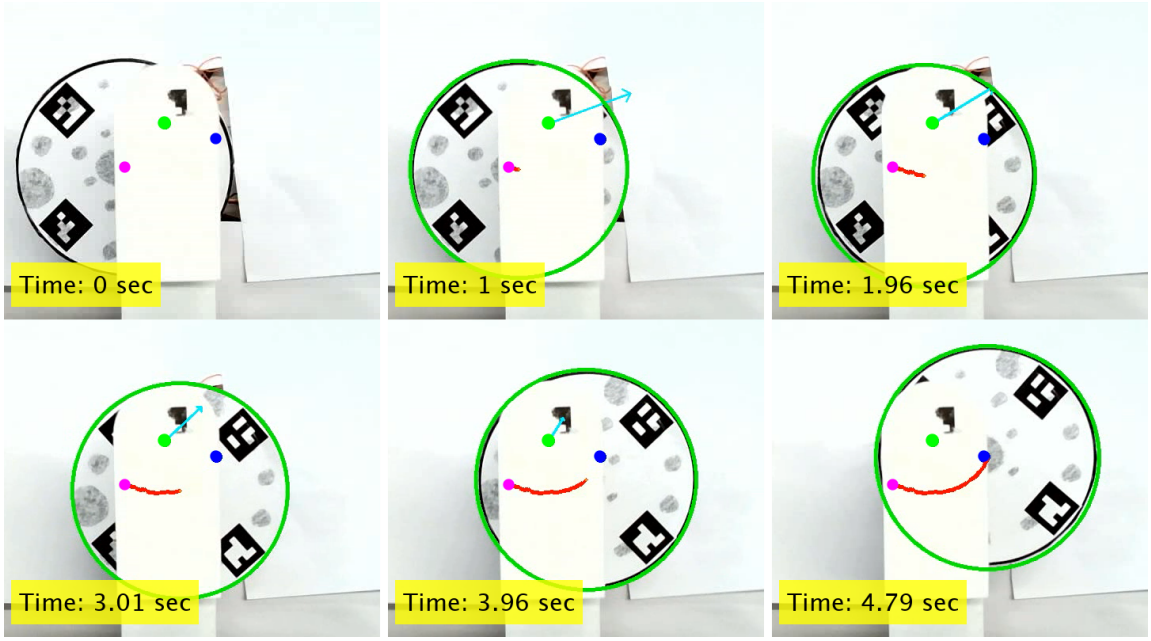

Figure 5.6: Manipulating the COM of a disk from an initial position (magenta marker) to a goal position (blue marker). The disk reached the goal with an accuracy of 1.93 mm error and 9.94^o orientation change.

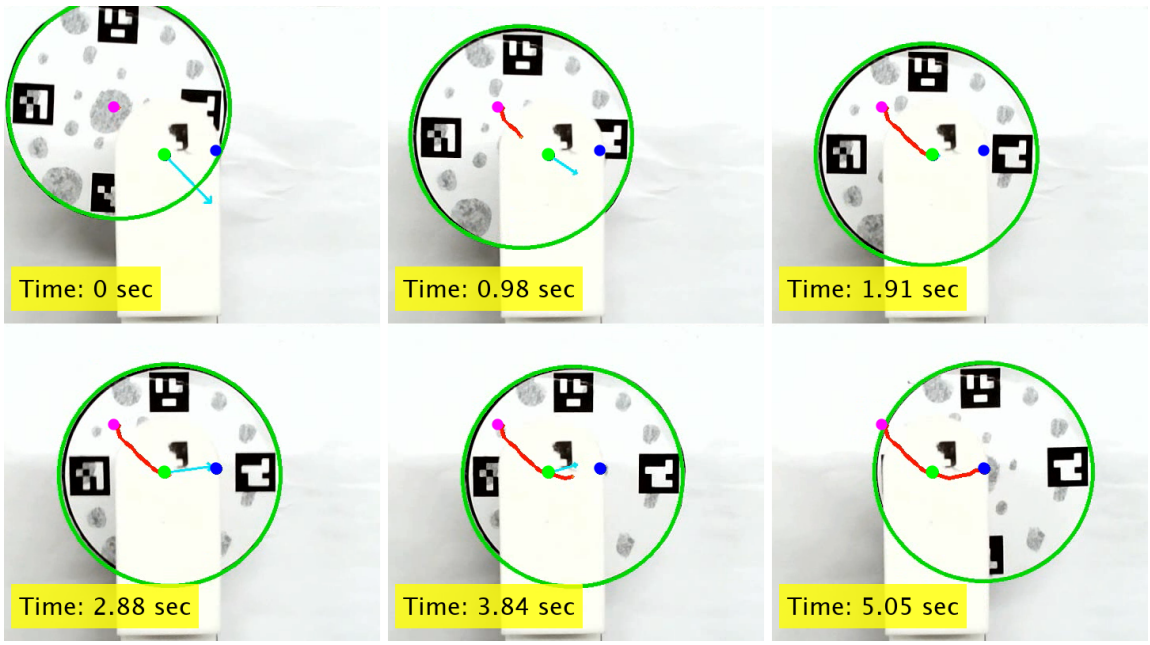

Figure 5.7: Manipulating the COM of a disk from an initial position (magenta marker) to a goal position (blue marker) through the origin (green marker). The disk reached the goal with an accuracy of 2 mm error and 4.39^o orientation change.

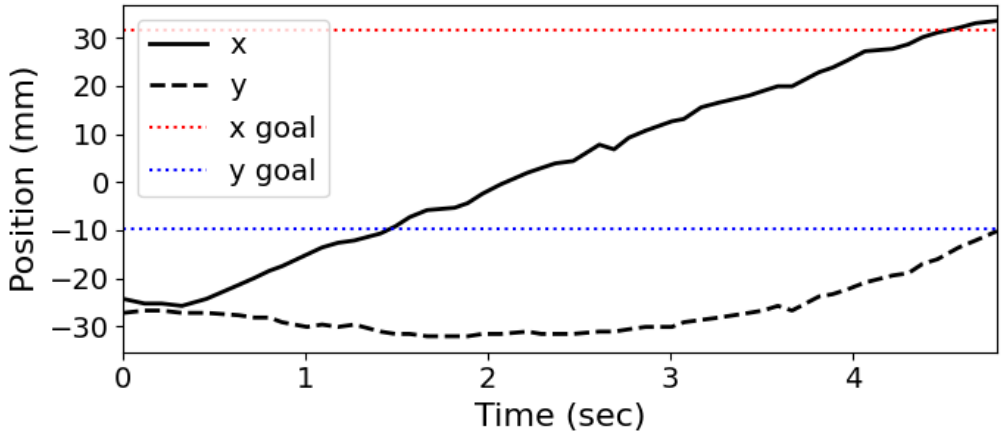

Figure 5.8: Position path of the disk seen in Figure 5.6 with respect to time.

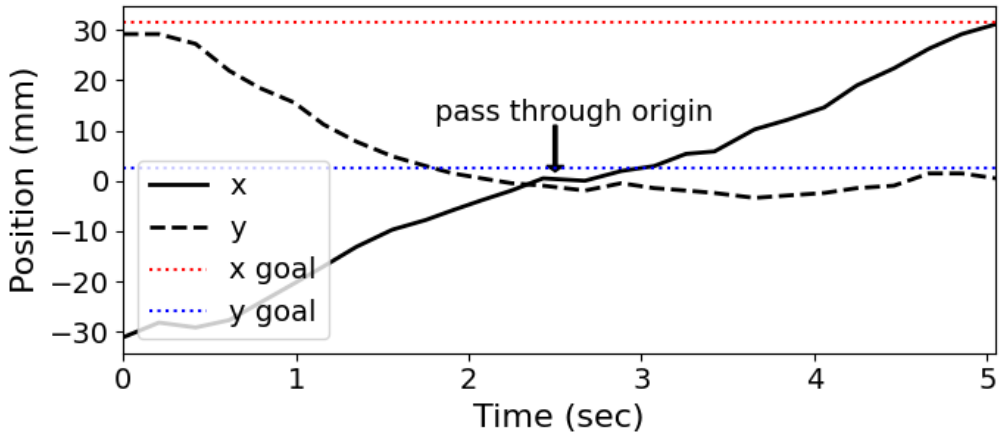

Figure 5.9: Position path of the disk seen in Figure 5.7 with respect to time.

Table 5.2: Tracking accuracy along a path

	Size (mm)	Tracking error (mm)
Rectangular	15×15	1.73±0.50
Circular	9 (radius)	1.99±0.31

Table 5.3: Performance parameters for various manipulated objects

Object	Thickness (mm)	Weight (g)	Velocity (mm/sec)	Accuracy (mm)
Utility Knife	0.2	4.68	9.7±1.22	2.01±0.38
Ruler	0.2	10.43	1.95±0.1	2.56±0.21
ID card	0.6	3.77	12.95±20.35	1.82±1.17
Paper sheet	0.05	0.71	1.41±1.55	2.5±0.2
Paperboard	0.1	1.00	1.84±1.39	2.15±0.59
Single wall cardboard	3.8	3.1	0	-

paths. Figures 5.10 and 5.11 show snapshots of tracking both paths. Results demonstrate the ability to track paths with high accuracy.

5.3.3 Other objects

To demonstrate the manipulation of various objects, six everyday objects were tested. The set of objects, seen in Figure 5.12, includes a stainless steel utility knife, a stainless Steel ruler, a plastic ID card, a paper sheet, a paperboard and a single wall cardboard. Weight and thickness of the objects along with experimental results are seen in Table 5.3. The results include mean and standard deviation for motion velocity and control error. The results show that smooth objects (i.e., utility knife and ID card) move faster than objects with rougher surface texture. Due to low kinetic friction, force f_c is stronger as seen in (4.9) yielding higher velocity. However, local deformation on the cardboard caused by gripper clamping prevented it from moving while only rotating about the contact point. In the control experiment, the attached marker on the object (not on the COM) was driven to ten desired goals showing good accuracy for all objects.

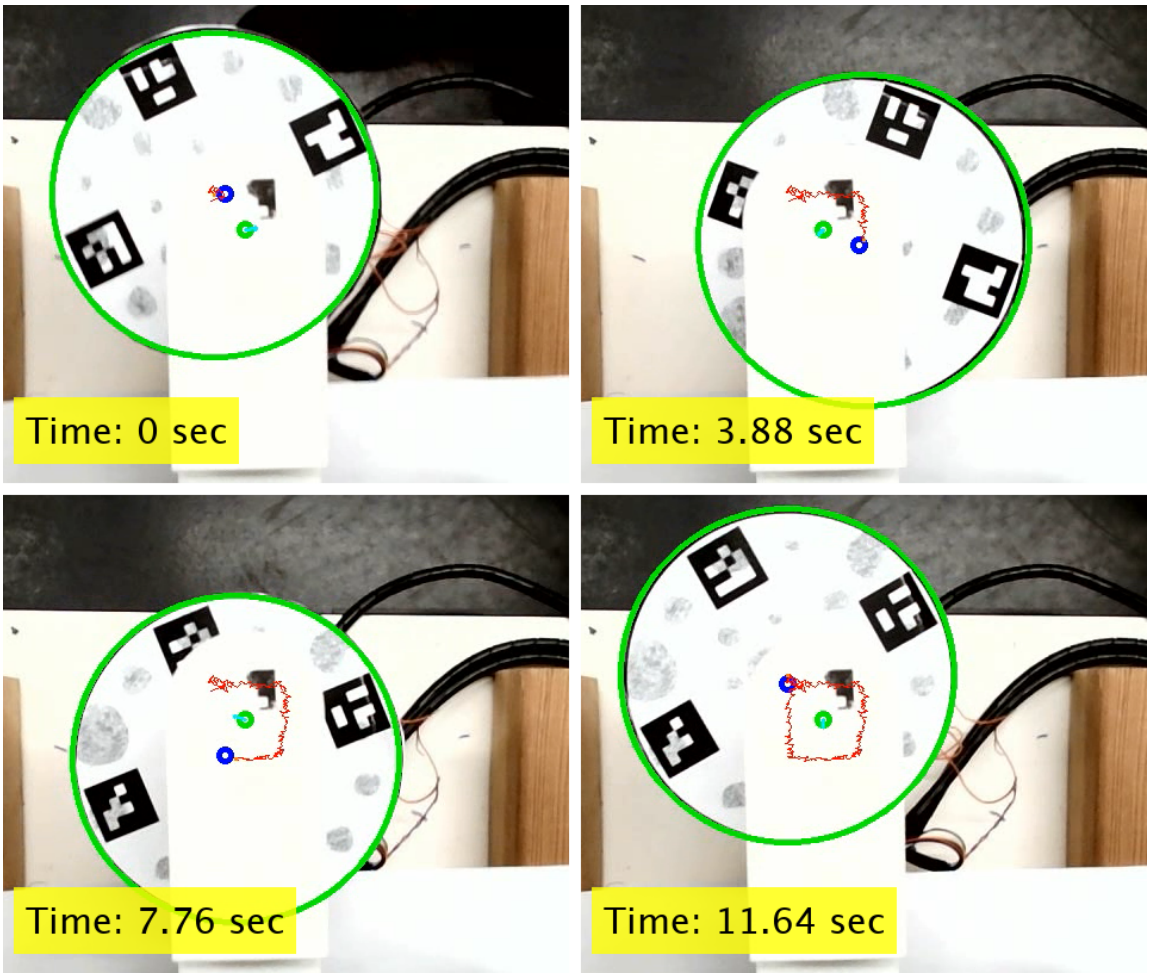

Figure 5.10: Manipulating the COM of a disk along a rectangular path (red path).

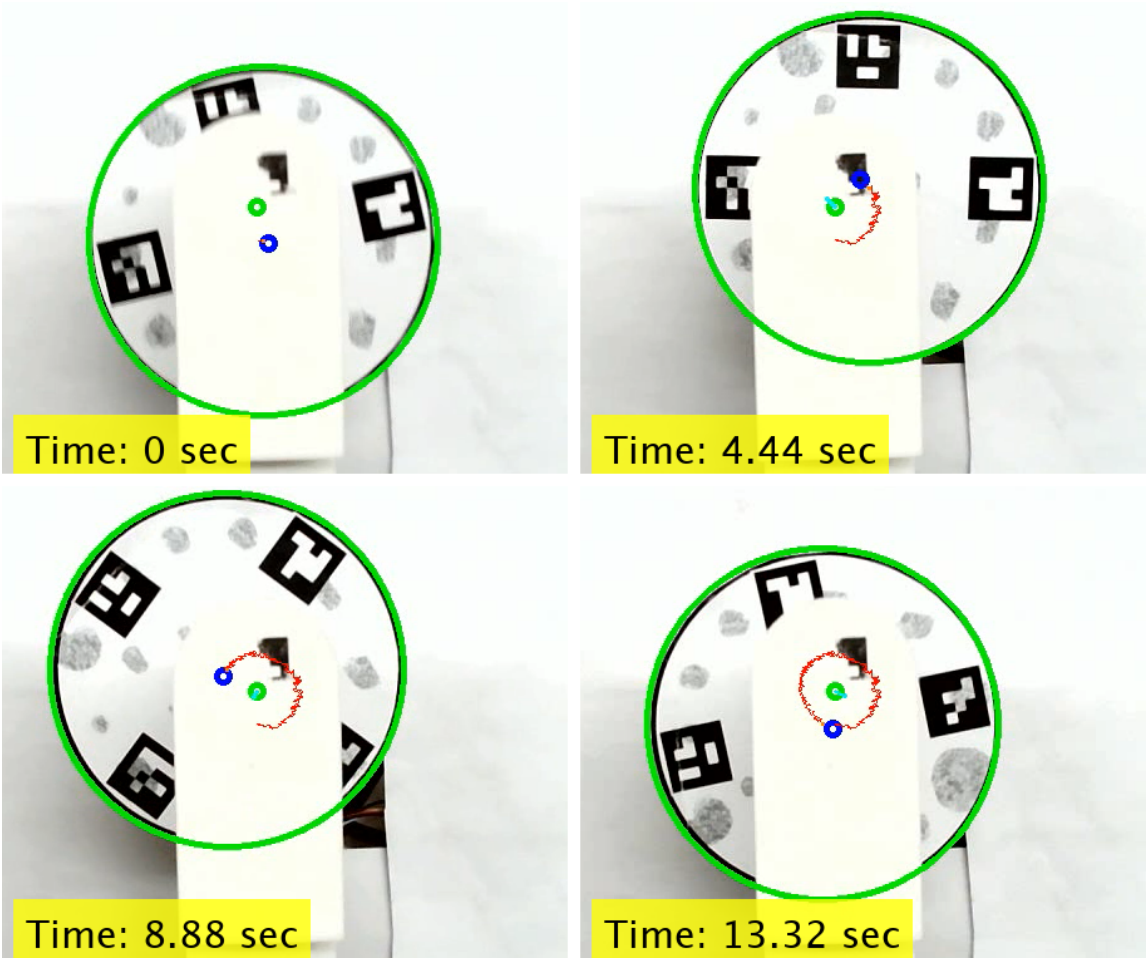

Figure 5.11: Manipulating the COM of a disk along a circular path (red path).

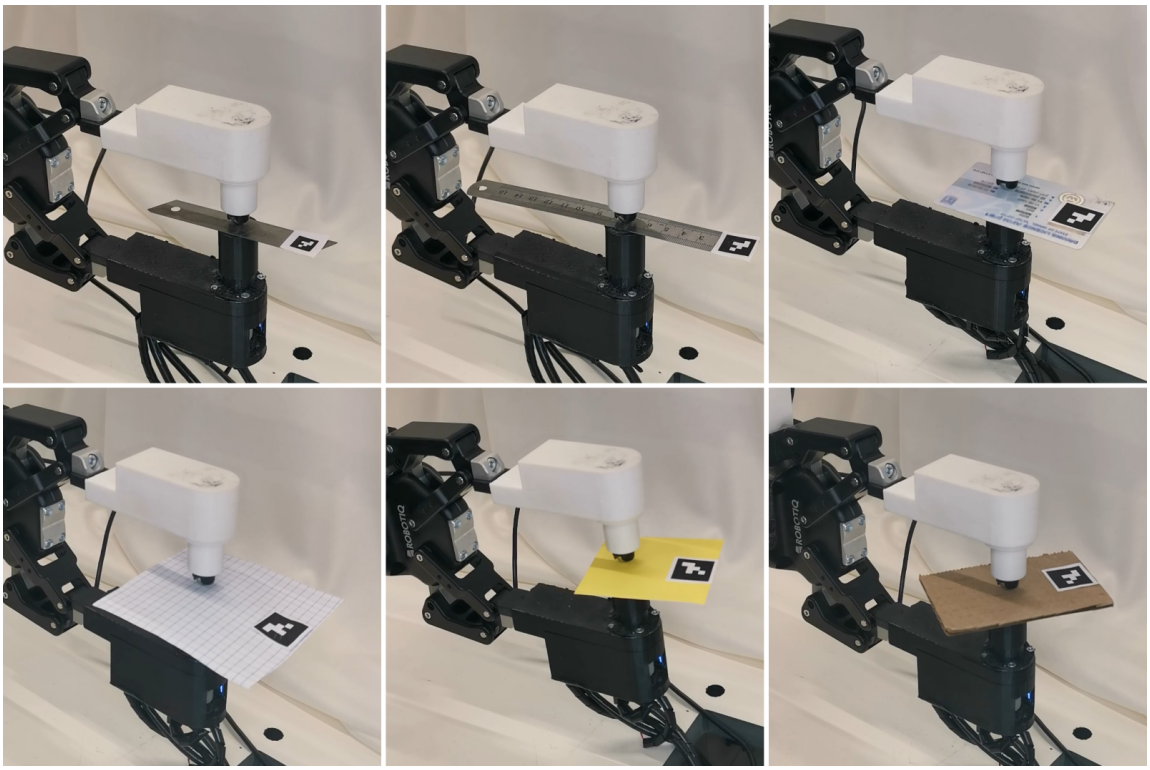

Figure 5.12: Manipulating various objects including (from top left): utility knife, ruler, ID card, paper sheet, paperboard and single wall cardboard.

6 Conclusions and Future Work

In this thesis work, a novel vibration-based mechanism was presented for in-hand manipulation of thin objects. The mechanism can augment parallel grippers which alone do not have intrinsic in-hand manipulation capabilities. The proposed mechanism is based on the stick-slip phenomenon yielding a simple and low-cost solution. By having a finger comprised of an off-the-shelf vibration motor and a rotary actuator, a force can be exerted on a grasped object in a desired direction. Then, by applying a simple control law, the object can be manipulated to a desired position goal or track a path with high accuracy. A set of experiments was presented including accuracy with regards to frequency and gripper inclination angle, control behaviour and manipulation of various objects. The results show high accuracy and feasibility to objects of different material and texture.

As discussed on Section 4.1.2, the proposed mechanism is underactuated and demonstrated the ability to control the position of the object. However, controlling the orientation of the object would require planned maneuvers while considering the applied torques. For instance, future work can apply a Model Predictive Control where a motion planner constantly plans paths to a goal in $SE(2)$ based on the dynamic model. Another alternative is a gravity-assisted approach where the object is pivoted with controlled inclination of the gripper. Future work may also consider identifying the multiple vibration modes of the system to better control the motion of various objects. Furthermore, the current sensing is limited by the accuracy of the ArUco markers while also dependent on camera line-of-sight. Hence, future work could consider an on-board sensing module that can combine visual perception and odometry. Adaptive velocity control may also be implemented to reduce the velocity when approaching the vicinity of the goal for finer position tuning. Future work can include another VFM model on the other finger thus, increasing the input of the system and maybe achieve also orientation control.

References

[1] *In-Hand Manipulation Primitives for a Minimal, Underactuated Gripper With Active Surfaces*, volume Volume 5A: 40th Mechanisms and Robotics Conference of *International Design Engineering Technical Conferences and Computers and Information in Engineering Conference*, 08 2016.

[2] B. Baksys, K. RamanauskytÄ, and A. Povilionis. Vibratory manipulation of elastically unconstrained part on a horizontal plane. *Mechanika*, 75(1), 2009.

[3] Aude Billard and Danica Kragic. Trends and challenges in robot manipulation. *Science*, 364(6446), 2019.

[4] Karl Böhringer, Vivek Bhatt, and Kenneth Goldberg. Sensorless manipulation using transverse vibrations of a plate. volume 2, pages 1989 – 1996, 1995. ISBN 0-7803-1965-6.

[5] J. Breguet and R. Clavel. Stick and slip actuators: design, control, performances and applications. In *Proceedings of the International Symposium on Micromechatronics and Human Science*, pages 89–95, 1998.

[6] Ian M. Bullock and Aaron M. Dollar. A two-fingered underactuated anthropomorphic manipulator based on human precision manipulation motions. In *2016 IEEE International Conference on Robotics and Automation (ICRA)*, pages 384–391, 2016. doi: 10.1109/ICRA.2016.7487157.

[7] Jayden Chapman, Gal Gorjup, Anany Dwivedi, Saori Matsunaga, Toshisada Mariyama, Bruce MacDonald, and Minas Liarokapis. A locally-adaptive, parallel-jaw gripper with clamping and rolling capable, soft fingertips for fine manipulation of flexible flat cables. In *IEEE International Conference on Robotics and Automation (ICRA)*, pages 6941–6947, 2021.

[8] Nikhil Chavan-Dafle, Matthew T. Mason, Harald Staab, Gregory Rossano, and Alberto Rodriguez. A two-phase gripper to reorient and grasp. In *2015 IEEE International Conference on Automation Science and Engineering (CASE)*, pages 1249–1255, 2015. doi: 10.1109/CoASE.2015.7294269.

[9] Nikhil Chavan-Dafle, Rachel Holladay, and Alberto Rodriguez. Planar in-hand manipulation via motion cones. *The International Journal of Robotics Research*, 39 (2-3):163–182, 2020.

[10] Yuan Chen, Colin Prepscius, Daewon Lee, and Daniel D. Lee. Tactile velocity estimation for controlled in-grasp sliding. *IEEE Robotics and Automation Letters*, 6(2): 1614–1621, 2021.

[11] E.F.F. Chladni. *Entdeckungen über die Theorie des Klanges*. Number 1. Bey Weidmanns erben und Reich, 1787.

[12] Marco Costanzo. Control of robotic object pivoting based on tactile sensing. *Mechatronics*, 76:102545, 2021. ISSN 0957-4158.

[13] Marco Costanzo, Giuseppe De Maria, and Ciro Natale. Dual-arm in-hand manipulation with parallel grippers using tactile feedback. In *International Conference on Advanced Robotics (ICAR)*, pages 942–947, 2021.

[14] Silvia Cruciani and Christian Smith. Integrating path planning and pivoting. In *IEEE/RSJ International Conference on Intelligent Robots and Systems (IROS)*, pages 6601–6608, 2018.

[15] Silvia Cruciani, Christian Smith, Danica Kragic, and Kaiyu Hang. Dexterous manipulation graphs. In *IEEE/RSJ International Conference on Intelligent Robots and Systems (IROS)*, pages 2040–2047, 2018.

[16] Nikhil Chavan Dafle, Alberto Rodriguez, Robert Paolini, Bowei Tang, Siddhartha S. Srinivasa, Michael Erdmann, Matthew T. Mason, Ivan Lundberg, Harald Staab, and Thomas Fuhlbrigge. Extrinsic dexterity: In-hand manipulation with external forces. In *2014 IEEE International Conference on Robotics and Automation (ICRA)*, pages 1578–1585, 2014. doi: 10.1109/ICRA.2014.6907062.

[17] Nikhil Chavan Dafle, Alberto Rodriguez, Robert Paolini, Bowei Tang, Siddhartha S. Srinivasa, Michael Erdmann, Matthew T. Mason, Ivan Lundberg, Harald Staab, and Thomas Fuhlbrigge. Extrinsic dexterity: In-hand manipulation with external forces. In *2014 IEEE International Conference on Robotics and Automation (ICRA)*, pages 1578–1585, 2014.

[18] Hamed Demaghsi, Hadi Mirzajani, and Habib Badri Ghavifekr. Design and simulation of a novel metallic microgripper using vibration to release nano objects actively. *Microsystem technologies*, 20(1):65–72, 2014.

[19] W. Y. Du and S. L. Dickerson. Modelling and control of a novel vibratory feeder. In *IEEE/ASME International Conference on Advanced Intelligent Mechatronics*, pages 496–501, 1999.

[20] Xing Gao, Chongjing Cao, Jianglong Guo, and Andrew Conn. Elastic electroadhesion with rapid release by integrated resonant vibration. *Advanced Materials Technologies*, 4(1):1800378, 2019.

[21] S. Garrido-Jurado, R. Munoz-Salinas, F.J. Madrid-Cuevas, and M.J. MarÃn-Jimenez. Automatic generation and detection of highly reliable fiducial markers under occlusion. *Pattern Recognition*, 47(6):2280–2292, 2014. ISSN 0031-3203.

[22] JianPo Guo, PeiZhang Wu, and WeiRu Wang. A precision pose measurement technique based on multi-cooperative logo. *Journal of Physics: Conference Series*, 1607 (1):012047, aug 2020.

[23] Menglong Guo, David V. Gealy, Jacky Liang, Jeffrey Mahler, Aimee Goncalves, Stephen McKinley, Juan Aparicio Ojea, and Ken Goldberg. Design of parallel-jaw gripper tip surfaces for robust grasping. In *2017 IEEE International Conference on Robotics and Automation (ICRA)*, pages 2831–2838, 2017.

[24] Katharina Hertkorn, Maximo A. Roa, and Christoph Borst. Planning in-hand object manipulation with multifingered hands considering task constraints. In *IEEE International Conference on Robotics and Automation*, pages 617–624, 2013.

[25] Satoshi Honda. Development of an intelligent vibration gripper. In George D. Foret, Kam C. Lau, and Bartholomew O. Nnaji, editors, *Machine Tool, In-Line, and Robot*

Sensors and Controls, volume 2595, pages 170 – 177. International Society for Optics and Photonics, 1995.

[26] Michail Kalaitzakis, Sabrina Carroll, Anand Ambrosi, Camden Whitehead, and Nikolaos Vitzilaios. Experimental comparison of fiducial markers for pose estimation. In *International Conference on Unmanned Aircraft Systems (ICUAS)*, pages 781–789, 2020.

[27] Dean Karnopp. Computer Simulation of Stick-Slip Friction in Mechanical Dynamic Systems. *Journal of Dynamic Systems, Measurement, and Control*, 107(1):100–103, 03 1985.

[28] Artur Kopitca, Kourosh Latifi, and Quan Zhou. Programmable assembly of particles on a chladni plate. *Science Advances*, 7(39):eabi7716, 2021.

[29] Zhili Long, Jianguo Zhang, Yuecai Liu, Cuihong Han, Yanle Li, and Zuohua Li. Dynamics modeling and residual vibration control of a piezoelectric gripper during wire bonding. *IEEE Transactions on Components, Packaging and Manufacturing Technology*, 7(12):2045–2056, 2017.

[30] Raymond Ma, Adam Spiers, and Aaron Dollar. M2 gripper: Extending the dexterity of a simple, underactuated gripper. volume 36, 07 2015. ISBN 978-3-319-23326-0. doi: 10.1007/978-3-319-23327-$7_6$8.

[31] Mohammad Mayyas. Parallel manipulation based on stick-slip motion of vibrating platform. *Robotics*, 9(4), 2020.

[32] Connor McCann, Vatsal Patel, and Aaron Dollar. The stewart hand: A highly dexterous, six-degrees-of-freedom manipulator based on the stewart-gough platform. *IEEE Robotics Automation Magazine*, 28(2):23–36, 2021. doi: 10.1109/MRA.2021.3064750.

[33] Kazuyuki Nagata. Manipulation by a parallel-jaw gripper having a turntable at each fingertip. In *IEEE International Conference on Robotics and Automation*, pages 1663–1670 vol.2, 1994.

[34] Keiichi Nakamura and Satoshi Honda. Development of multifinger robot hand with vibration fingers. In George D. Foret, Kam C. Lau, and Bartholomew O. Nnaji, editors, *Machine Tool, In-Line, and Robot Sensors and Controls*, volume 2595, pages 214 – 218. International Society for Optics and Photonics, SPIE, 1995.

[35] Vatsal Patel and Aaron Dollar. Robot hand based on a spherical parallel mechanism for within-hand rotations about a fixed point. pages 709–716, 09 2021. doi: 10.1109/IROS51168.2021.9636704.

[36] D. Reznik and J. Canny. A flat rigid plate is a universal planar manipulator. In *Proceedings IEEE International Conference on Robotics and Automation*, volume 2, pages 1471–1477 vol.2, 1998.

[37] Weibin Rong, Zenghua Fan, Lefeng Wang, Hui Xie, and Lining Sun. A vacuum microgripping tool with integrated vibration releasing capability. *Review of Scientific Instruments*, 85(8):085002, 2014.

[38] Michael Rubenstein, Christian Ahler, Nick Hoff, Adrian Cabrera, and Radhika Nagpal. Kilobot: A low cost robot with scalable operations designed for collective behaviors. *Robotics and Autonomous Systems*, 62(7):966 – 975, 2014.

[39] Michael Rubenstein, Alejandro Cornejo, and Radhika Nagpal. Programmable self-assembly in a thousand-robot swarm. *Science*, 345(6198), 2014.

[40] Ferdinand Schmoeckel and Sergej Fatikow. Smart flexible microrobots for scanning electron microscope (sem) applications. *Journal of Intelligent Material Systems and Structures*, 11(3):191–198, 2000.

[41] Jian Shi, J. Zachary Woodruff, Paul B. Umbanhowar, and Kevin M. Lynch. Dynamic in-hand sliding manipulation. *IEEE Transactions on Robotics*, 33(4):778–795, 2017.

[42] V. Shrikanth, K. R. Y. Simha, and M. S. Bobji. Frictional force measurement during stick-slip motion of a piezoelectric walker. In *IEEE International Conference on Industrial Technology*, pages 1463–1468, 2015.

[43] Avishai Sintov and Amir Shapiro. Swing-up regrasping algorithm using energy control. In *IEEE International Conference on Robotics and Automation (ICRA)*, pages 4888–4893, 2016.

[44] Avishai Sintov and Amir Shapiro. Dynamic regrasping by in-hand orienting of grasped objects using non-dexterous robotic grippers. *Robotics and Computer-Integrated Manufacturing*, 50:114 – 131, 2017. ISSN 0736-5845.

[45] Avishai Sintov, Or Tslil, and Amir Shapiro. Robotic swing-up regrasping manipulation based on the impulseâmomentum approach and clqr control. *IEEE Transactions on Robotics*, 32(5):1079–1090, 2016.

[46] Avishai Sintov, Or Tslil, and Amir Shapiro. Robotic swing-up regrasping manipulation based on impulse-momentum approach and cLQR control. *IEEE Transactions on Robotics*, 32(5):1079–1090, 2016.

[47] J.J.E. Slotine and W. Li. *Applied Nonlinear Control*. Prentice Hall, 1991. ISBN 9780130408907.

[48] Adam J. Spiers, Berk Calli, and Aaron M. Dollar. Variable-friction finger surfaces to enable within-hand manipulation via gripping and sliding. *IEEE Robotics and Automation Letters*, 3(4):4116–4123, 2018. doi: 10.1109/LRA.2018.2856398.

[49] Yoshiyuki Suzuki, Akihiko Yamaguchi, Seita Nojiri, Tetsuyou Watanabe, and Koichi Hashimoto. Vibration control for pivoting by robot hand equipped with cavs and fingervision. In *2021 Fifth IEEE International Conference on Robotic Computing (IRC)*, pages 18–26, 2021.

[50] Ian H. Taylor, Nikhil Chavan-Dafle, Godric Li, Neel Doshi, and Alberto Rodriguez. Pnugrip: An active two-phase gripper for dexterous manipulation. In *IEEE/RSJ International Conference on Intelligent Robots and Systems (IROS)*, pages 9144–9150, 2020.

[51] Hajime Terasaki and Tsutomu Hasegawa. Motion planning of intelligent manipulation by a parallel two-fingered gripper equipped with a simple rotating mechanism. *IEEE Transactions on Robotics and Automation*, 14(2):207–219, 1998.

[52] Vinicio Tincani, Manuel G. Catalano, Edoardo Farnioli, Manolo Garabini, Giorgio Grioli, Gualtiero Fantoni, and Antonio Bicchi. Velvet fingers: A dexterous gripper with active surfaces. In *2012 IEEE/RSJ International Conference on Intelligent Robots and Systems*, pages 1257–1263, 2012. doi: 10.1109/IROS.2012.6385939.

[53] Sho Tsuchiya, Masashi Konyo, Hiroshi Yamada, Takahiro Yamauchi, Shogo Okamoto, and Satoshi Tadokoro. Vib-touch: Virtual active touch interface for handheld devices. In *RO-MAN 2009 - The 18th IEEE International Symposium on Robot and Human Interactive Communication*, pages 12–17, 2009. doi: 10.1109/ROMAN.2009.5326160.

[54] Takuya Umedachi, Vishesh Vikas, and Barry A. Trimmer. Highly deformable 3-d printed soft robot generating inching and crawling locomotions with variable friction legs. In *2013 IEEE/RSJ International Conference on Intelligent Robots and Systems*, pages 4590–4595, 2013. doi: 10.1109/IROS.2013.6697016.

[55] P. Vartholomeos and E. Papadopoulos. Analysis, design and control of a planar micro-robot driven by two centripetal-force actuators. In *Proceedings IEEE International Conference on Robotics and Automation*, pages 649–654, 2006.

[56] P. Vartholomeos, K. Mougiakos, and E. Papadopoulos. Driving principles and hardware integration of microrobots employing vibration micromotors. In *IEEE/ASME international conference on advanced intelligent mechatronics*, pages 1–6, 2007.

[57] Francisco E. Vina B., Yiannis Karayiannidis, Karl Pauwels, Christian Smith, and Danica Kragic. In-hand manipulation using gravity and controlled slip. In *2015 IEEE/RSJ International Conference on Intelligent Robots and Systems (IROS)*, pages 5636–5641, 2015. doi: 10.1109/IROS.2015.7354177.

[58] Francisco E. ViÃ±a B., *YiannisKarayiannidis*, *KarlPauwels*, *ChristianSmith*, *andDanicaKragic*. *In−handmanipulationusinggravityandcontrolledslip*. *InIEEE/RSJ International Conference on Intelligent* −5641, 2015.

[59] Francisco E. ViÃ±a B., *YiannisKarayiannidis*, *ChristianSmith*, *andDanicaKragic*. *Adaptivecontrol for* −406, 2016.

[60] V.I. Vorotnikov. On the theory of partial stability. *Journal of Applied Mathematics and Mechanics*, 59(4):525–531, 1995. ISSN 0021-8928.

[61] Daniel E. Welcome, Ren G. Dong, Xueyan S. Xu, Christopher Warren, and Thomas W. McDowell. The effects of vibration-reducing gloves on finger vibration. *International Journal of Industrial Ergonomics*, 44(1):45–59, 2014. ISSN 0169-8141.

[62] Andy Zeng, Shuran Song, Kuan-Ting Yu, Elliott Donlon, Francois R. Hogan, Maria Bauza, Daolin Ma, Orion Taylor, Melody Liu, Eudald Romo, Nima Fazeli, Ferran Alet, Nikhil Chavan Dafle, Rachel Holladay, Isabella Morena, Prem Qu Nair, Druck Green, Ian Taylor, Weber Liu, Thomas Funkhouser, and Alberto Rodriguez. Robotic pick-and-place of novel objects in clutter with multi-affordance grasping and cross-domain image

matching. In *IEEE International Conference on Robotics and Automation (ICRA)*, pages 3750–3757, 2018.

[63] Jie Zhao, Xin Jiang, Xiaoman Wang, Shengfan Wang, and Yunhui Liu. Assembly of randomly placed parts realized by using only one robot arm with a general parallel-jaw gripper. pages 5024–5030, 2020.

[64] Q. Zhou, V. Sariola, K. Latifi, and Ville Liimatainen. Controlling the motion of multiple objects on a chladni plate. *Nature Communication*, 7(12764), 2016.

[65] Shiping Zuo, Jianfeng Li, and Mingjie Dong. Design, modeling, and manipulability evaluation of a novel four-dof parallel gripper for dexterous in-hand manipulation. *Journal of Mechanical Science and Technology*, 35:1–16, 06 2021.

תקציר

מניפולציה תוך יד מתייחסת לאינטראקציות של רובוטים עם החפצים שהם מחזיקים. זה כולל איך הרובוט תופס, שולט ומתמרן אובייקטים. אינטראקציות כאלה דורשות תכנון ועיצוב של מערכות מורכבות. נושא זה הוא אחד הנושאים הנחקרים ביותר בתחום הרובוטיקה כאשר ישנן שיטות שונות לתפעול חפצים תוך שימוש ביד רובוטית בדרגות חופש מרובות או בידיים רובוטיות גמישות. עם זאת, תפסניות מקבילות סובלות מהיעדר דרגות חופש ולכן מוגבלות לסגירה על אובייקט בלבד ללא יכולת מניפולציה פנימית ביד. עם זאת, תפסנים מקבילים נמצאים בשימוש נרחב בשל פשטותם והעלות הנמוכה שלהם תוך הסתמכות על יכולות חיצוניות לתפעול האובייקט.

בעבודה זו, מוצע מנגנון פשוט ובעלות נמוכה לתת את להקנות לתפסנית מקבילה יכולות לבצע מניפולציה פנימיות ביד. בעבודה זו מוצעת אצבע חדשנית מבוססת רטט שבה מנוע מסה מסתובב אקסצנטרי מהמדף יחד עם מנוע סיבובי פשוט מפעילים כוחות תנועה על חפץ דק שנתפס. התנועה מבוססת על תופעת הדבקה החלקה (Slip Stick) ומופעלת ללא חלקים נעים חשופים. יחד עם המנגנון, מוצעים חוקי בקרה פשוטים כדי לתמרן את האובייקט ליעדי מיקום רצויים ולאורך נתיבים. יתר על כן, מודגמת היכולת לתפעל אובייקטים שונים. תוצאות ניסוי מראות את היכולת לתפעל אובייקט בדיוק של פחות מ-2~ מ״מ.הניסויים מדגימים את היתרונות של הגישה המעניקה יכולות מניפולציה ביד, שבעבר לא היו אפשריות, לתפסנית מקבילה.

אוניברסיטת תל אביב
הפקולטה להנדסה ע״ש איבי ואלדר פליישמן
בית הספר לתארים מתקדמים ע״ש זנדמן סליינר

מניפולציות תוך יד באמצעות תפסנית רובוטית עם אצבעות רטט

חיבור זה הוגש כעבודת מחקר לקראת התואר ״מוסמך אוניברסיטה״ בהנדסה מכנית
על ידי

נועם נחום

העבודה נעשתה בבית הספר להנדסה מכנית
בהנחיית ד״ר אבישי סינטוב

אב תשפ״ב